Thermoeconomic and optimization analyses of direct oxy-combustion supercritical carbon dioxide power cycles with dry and wet cooling

Ahmad K. Sleiti [a,*], Wahib A. Al-Ammari [a], Ladislav Vesely [b], Jayanta S. Kapat [b]

[a] *Department of Mechanical & Industrial Engineering, College of Engineering, Qatar University, Doha, Qatar*
[b] *Department of Mechanical and Aerospace Engineering, Center for Gas Turbines and Energy Research (CATER), University of Central Florida, Orlando, FL, USA*

ARTICLE INFO

ABSTRACT

Oxy-combustion supercritical CO_2 power cycles have the advantages of high-energy efficiency and near-zero pollutant emissions. Thus, these cycles are considered as an efficient way to reduce CO_2 emissions while maintaining economic growth. The major drawbacks of this technology include the lack of validated levelized cost of electricity (LCOE) studies; lower turbine inlet temperatures studies to accommodate the integration of various energy sources; solutions for the thermodynamic imbalance of the regenerator; and investigating the dry-versus the wet-cooling methods. These drawbacks are addressed in this paper by presenting comprehensive thermoeconomic and optimization analyses for three direct oxy-fuel sCO2 power cycles in wet and dry-cooling conditions. The first cycle M1 is a direct oxy-fuel sCO2 power cycle without preheater, the second cycle M2 integrates a preheater in parallel with the low-temperature recuperator of M1 while the third cycle M3 integrates a preheater in parallel with the high and low-temperature recuperators of M1. Results show that the integration of the preheater improves the thermal efficiency of M2 by 5.81% (wet), and 3.27% (dry), and of M3 by 13.27% (wet), and 6.58% (dry). The LCOE of M1 (without preheater) is higher than that of M2 by 10.8% (wet), and 5.7% (dry), and of M3 by 19.1% (wet), and 11.4% (dry). A minimum LCOE of 4.667¢/kWh$_e$ is obtained for M3 (wet) and of 6.139¢/kWh$_e$ for M3 (dry). At higher waste heat source temperature of 700 °C, the overall efficiency is improved by an average of 11% and the LCOE is reduced by 1.43 ¢/kWh$_e$.

1. Introduction

Over the past 50 years, global energy consumption has been rising due to population growth and the continuous evolution of the world's industrial, commercial and residential sectors. Simultaneously, the emissions of carbon dioxide (CO_2) and other harmful pollutants have been increasing by the burning of fossil fuels that provide about 80% of the global energy [1–3]. Owing to the global concerns of climate change, political and technological focus is now on minimizing CO_2 emissions [4]. Therefore, decarbonization technologies have gained much attention in recent years [5]. There are various approaches to minimize CO_2 emissions including 1) increasing the energy efficiency of the existing fossil-fuel power plants, 2) utilizing and integrating renewable energy sources (especially as an energy source for supercritical carbon dioxide (sCO2) power cycles [6–9]), and 3) developing innovative power cycles such as the closed power cycles with direct oxy-fuel combustion [10–12]. The first approach could reduce the growth of the CO_2 concentration in the air, however, it cannot maintain stable concentration

since the combustion products are still discharged into the atmosphere. The second approach is a promising solution, but it is only contributing by less than 5% (excluding the hydropower industry) to the total power structure. That is due to the high cost of energy storage and the complexity of power loading control [13]. The third approach (oxy-combustion technology) has the advantages of high energy efficiency and near-zero pollutant emissions [14]. This implies an efficient way to reduce CO_2 emissions while maintaining economic growth and hence is the focus of the present study.

Several oxy-combustion power cycles have been proposed over the past few decades such as the MATIANT (contraction of the names of the two designers MAThieu and IANTovski) cycle [15], the Graze cycle [16], the semi-closed oxy-combustion combined cycle (SCOC-CC) [17], and Allam cycle [18]. Currently, the Allam cycle is one of the most promising direct oxy-fuel power cycles, which can capture 98.9% of the combustion products with a net energy efficiency of 51.44% for gasified coal and 58.9% for natural gas [19,20]. However, the very high pressure (300 bar) and temperature (1150 °C) of the Allam cycle make the design of its components quite challenging and costly [21]. In particular, the

Nomenclature

Symbols

A	heat transfer area, (m^2)
$\dot{E}$	exergy rate, (kW)
f	temperature correction factor of the cost correlations
h	specific enthalpy, (kJ/kg)
$\dot{m}$	mass flow rate, (kg/s)
$\dot{n}$	molar flow rate, (kmol/s)
n	lifetime of the plant, (years)
P	pressure, (bar)
$\dot{Q}$	heat transfer rate, (kW)
R	gas constant, (kJ/kg-K)
S_r	split ratio
T	temperature, (°C & K)
U	overall heat transfer coefficient, (kW/m^2-°C)
$\dot{W}$	power produced or consumed by a layout component, (kW)
x_j	molar fraction
Z	component cost, ($, in 2019)
η	energy, mechanical, or isentropic efficiency, (%)
ε	exergy efficiency, (%)
φ	specific exergy, (kJ/kg)

Subscripts

1, 2, 3, …	state points as shown in Fig. 1, Fig. 2 and Fig. 3
ch	chemical
CO_2	produced carbon dioxide at the outlet of the combustor
DTS	depreciation tax shield
f	fuel (methane)
F,k	fuel exergy of component k
g	generator
h	for the high pressure at state (7)
i	Inlet
LOC	lifetime operating costs
L,k	loss exergy
l	for the low pressure at state (6)

max	maximum
net	net output
o	outlet (also ambient)
overall	for the overall exergy efficiency of the cycle
P,k	product exergy
ph	physical
rCO$_2$	recycled carbon dioxide to the combustor
th	for the thermal efficiency of the cycle (without the preheater load)
th,overall	the overall thermal efficiency of the cycle including the preheater load

Acronyms

ASU	air separation unit
CT	cooling tower
DP	depreciation period
DPC	dry precooler
DR	discount rate
FC	fuel compressor
GC	gas compressor
GT	gas turbine
HTR	high temperature recuperator
LCOE	levelized cost of electricity
LEP	lifetime electrical production
LHV	lower heating value
LTR	low temperature recuperator
MOF	Multi-objective function
OC	oxygen compressor
OMC	operating and maintenance cost
PH	preheater
PUF	plant utilization factor
PV	present value
SOF	Single objective function
sCO$_2$	supercritical carbon dioxide
TR	tax rate
WPC	water precooler
WS	water separator

regenerator has to handle five cold and hot streams including the turbine exhaust flow, the recycled sCO$_2$ flow, the oxidant, the turbine coolant flow, and the flow that transfers heat from the air separation unit (ASU) to the regenerator to correct the thermodynamic imbalance that occurs in the regenerator. This dictates an extremely large heat transfer area and robust structure to withstand the pressure differences (200–300 bar) and high temperatures (700–750 °C) [22].

Several studies have been conducted in open literature on the Allam cycle to evaluate its technical, environmental, and economical characteristics and to optimize the operating conditions of its components. In 2013, Allam et al. [23] demonstrated the features, technical characteristics, and challenges of their proposed cycle and then updated their demonstration in 2017 [24]. In 2016, Scaccabarozzi et al. [21] performed in-depth thermodynamic analysis and numerical optimization for the Allam cycle arriving at some optimized operating conditions for maximizing the cycle energy efficiency and recommended further techno-economic optimization for future work. Moreover, their results were reported only for the wet cooling conditions (T_{min} = 27 °C) at extremely high turbine inlet temperature (T_{max} = 1150 °C). In 2019, Rogalev et al. [25] performed equipment development study alongside thermodynamic optimization for the Allam cycle. They stressed that oxygen purity should not be higher than 91% to minimize the power consumed by the ASU and they proposed a single flow, double casing construction for the developed sCO$_2$ gas turbine. Economically, they only reported the total specific investment cost of the Allam cycle (1308

$/kW) at an assumed net output power of 100 MW and 30 years of operation. Also, in 2019, Zhu et al. [26] presented a modified Allam cycle without compressors at turbine inlet temperature between 600 °C and 900 °C and condensation temperature of 30 °C. Under the same operating conditions, they claimed that the energy efficiency of their modified cycle is higher than the original Allam cycle by 2–3%. However, their proposed modified cycle still needs economic assessment as it requires a liquified natural gas at cryogenic temperature (-162 °C) and low pressure (1 bar). In 2020, Chan et al. [27] introduced a novel layout of the Allam cycle by integrating a reheating system to the original Allam cycle. Based on their thermodynamic and optimization analysis, they found that the thermal efficiency of the novel cycle is lower than that of the original Allam cycle, however, the net power output of their cycle is about 2.2 times higher. Advanced control strategies for the Allam cycle to adjust the cycle loads at off-design conditions were introduced by Zaryab et al. [28]. However, further studies are needed to address the part-load efficiency maps of the air separation unit. Also, a more accurate model is needed for the assessment of the expansion efficiency losses at the part-load of the turbine. Recently, in 2021, Yu et al. [29] studied the Allam cycle with liquified natural gas (LNG) as a fuel to use its cold energy to minimize the compression power of the recycled and exported sCO$_2$. They studied various ways to utilize the cold energy of the LNG for a stand-alone power plant and a cogeneration system. They mentioned that the organic Rankine cycle cogeneration scheme is the best choice in terms of exergy efficiency. However, a detailed

techno-economic analysis is needed to make sure that the capital investment is within the reasonable range. Other studies related to the Allam cycle were recently presented focusing on the specific design of its multi-stream heat exchanger [30], its sensitivity analysis for the operational parameters [31], and its operation with LNG [32].

From an economic point of view, only a few papers have conducted economic analyses for oxy-direct combustion-based power systems. Ferrari et al. [33] presented technical and economic analyses for four oxy-turbine plants including semi-closed oxy-combustion combined cycle (SCOC-CC), NET power cycle, Graz cycle, and the Clean Energy System (CES) cycle. They reported that the LCOE of these four cycles are 0.105$/kWh, 0.094$/kWh, 0.106$/kWh, and 0.107$/kWh, respectively, at an operating life of 25 years, a capacity factor of 90%, and a discount rate of 8%. They stated that there is significant uncertainty in the estimated costs of the innovative equipment used in these cycles. Hervas et al. [34], introduced an exergoeconomic and economic of the basic Allam cycle and stated that its LCOE is 0.103$/kWh. However, the results were reported only for a single set of the operating parameters without sensitivity analyses on the effects of the variation of these parameters on the economic results. Also, the methods of calculating the capital cost of each cycle component were not stated in their study. Chan et al. [35] conducted thorough exergoeconomic and optimization analyses of the Allam cycle integrated with liquefied natural gas regasification process. However, they did not assess their system in terms of the LCOE. Alenezi et al. [36] performed an exergoeconomic analysis of the Allam-based cycle integrated with concentrated solar power as a major heat source. However, the exergoeconomic results were reported for the standalone configurations while the analysis of the hybrid configuration was recommended for future work. Except for Alenezi et al. [36], the previous economic studies were conducted at extremely high inlet turbine temperatures. In addition, they have not investigated or optimized the main operating conditions of their cycles at different cooling methods conditions, which is an important research gap that is addressed in the present study.

Furthermore, studies that have been performed for the Allam cycle mostly limit the design point to that mentioned by the cycle developers without investigating its performance at moderate turbine temperatures similar to those, for example, of the molten salt solar tower sCO_2 power systems (550–750 °C) [37,38]. These moderate-level temperatures are important to tap the potential of integrating the sCO_2 power cycles with concentrated solar power (CSP) technology, [39]. Moreover, to avoid the thermodynamic imbalance of the regenerator and to simplify the design requirements of the cycle components, other reliable solutions should be introduced rather than the heat recovery from the ASU. To address these drawbacks, Sleiti et al. [40] proposed direct oxy-fuel sCO_2 power cycles that integrate a preheater in parallel with the cycle's recuperator to correct the thermodynamic imbalance (that appears in the regenerator of the Allam cycle) and to minimize the consumed fuel by the combustor. However, they analyzed these configurations only with dry-cooling conditions. The dry-cooling process, however, could be implemented if the compression process is only performed by a gas compressor [41]. In many arid and desert regions in the world, where the ambient temperature is very high, the dry-cooling approach is not sufficient and the wet- or hybrid-cooling is unavoidable. Adding to that the factors of scarcity of water in such regions and its high cost [42,43], it is apparent that thorough research is still needed for the thermodynamic and economic evaluation of sCO_2 cycles with both wet- and dry-cooling configurations, which is one of the major goals of the present study. Furthermore, the LCOE of these configurations in the aforementioned study investigated the price of the waste heat at a single design point only. However, further economic analyses of these configurations with wide range of operating conditions and power capacity of each configuration (in wet and dry-cooling) are needed. Such analysis is a major step to decide the more efficient operational mode (wet or dry) in light of the economic feasibility of each configuration. Moreover, the study in [40] lacks the optimization analyses for these configurations,
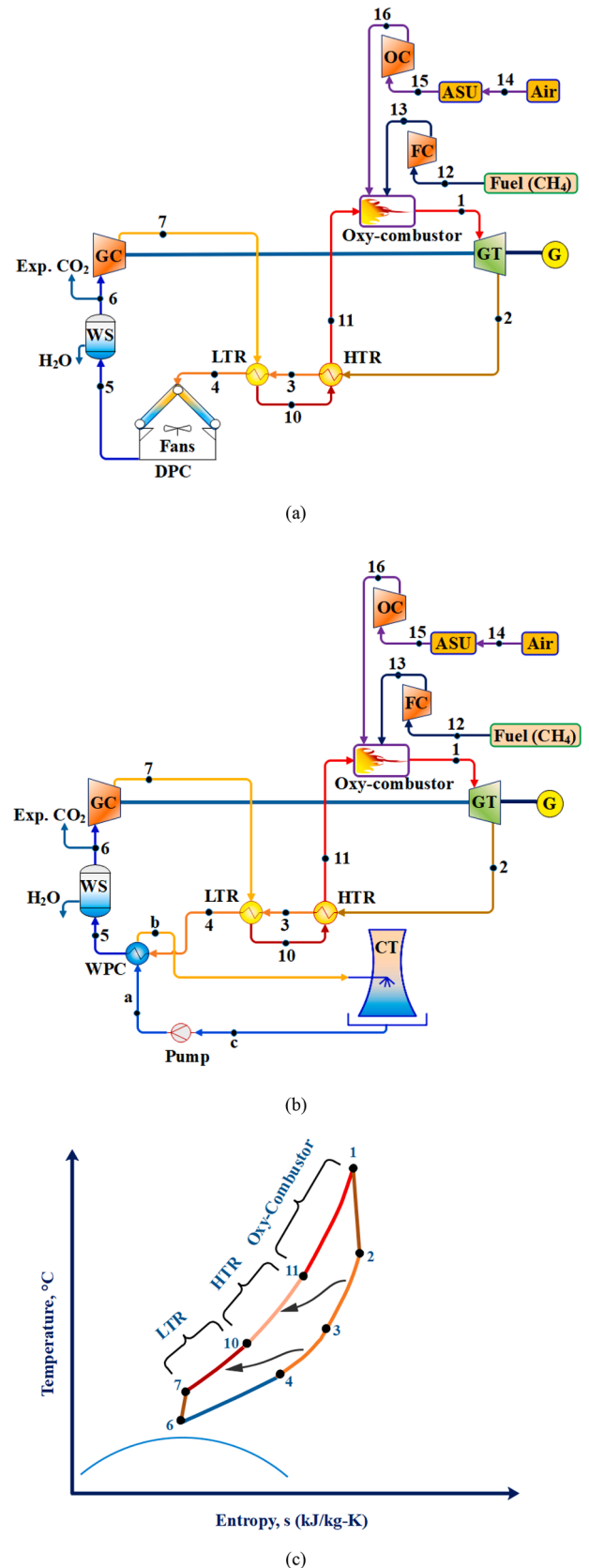

Fig. 1. Basic layout configuration (M1) of the direct oxy-combustor cycle. (a) dry-cooling, (b) wet-cooling processes without preheater, (c) T-s diagram.

which is crucial to identify the optimal operating conditions for each configuration. To fulfil all of these research gaps, the present study is aiming at the following:

- Comprehensively evaluating the performance of the proposed configurations from energetic, exergetic, and economic points of view in wet and dry-cooling conditions.
- Providing guidelines for detailed LCOE analysis of sCO_2 power cycles based on the most current costs of components and operation.
- Comparing and optimizing the performance of the proposed configurations under the wet and dry-cooling conditions.
- Identifying the optimal operating conditions for each configuration based on single- and multi-objective optimization analyses.

To realize these aims, the present study represents the three sCO_2 power cycle configurations proposed by the authors in Sleiti et al. [40] with addition of wet cooling, detailed LCOE analysis, multi-objective optimization and thorough comparison of wet versus dry cooling configurations. The basic cycle configuration (M1), as a reference layout, consists mainly of a direct oxy-combustor, gas turbine, gas compressor, precooler, low-temperature recuperator (LTR), and high-temperature recuperator (HTR) without preheater. The second configuration (M2) involves the same components in addition to a preheater integrated in parallel with the LTR to improve the PIs. The third configuration integrates the preheater in parallel with both the LTR and the HTR.

The rest of the manuscript is organized into four more sections. Section 2 describes the proposed configurations detailing their technical characteristics and advantages. Section 3 presents the developed energetic, exergetic, and economic models and the validation results. In section 4, parametric studies are carried out for the major operating conditions including the split ratio, maximum and minimum cycle temperatures, pressures, and waste heat source temperature. The results of the single- and multi-objective optimization analysis are presented and discussed in subsection 4.6 with a comparison of the minimum LCOE obtained by the multi-objective optimization in the present study to similar configurations available in the literature. The main findings, conclusions and future work are summarized in section 5.

2. Description of sCO_2 cycle configurations

The basic configuration of the direct oxy-combustor sCO_2 power cycle (M1) is shown in Fig. 1 (a, b) with T-s diagram in Fig. 1c. Fig. 1(a) shows M1 equipped with a dry precooler (DPC), while Fig. 1(b) shows M1 equipped with a wet precooler (WPC). The other components, which are the oxy-combustor, gas turbine (GT), gas compressor (GC), high-temperature recuperator (HTR), low-temperature recuperator (LTR), water separator (WS), air separation unit (ASU), oxygen compressor (OC), and fuel compressor (FC), are the same in both dry and wet-cooling configurations. Bearing in mind the difference in the cooling method (dry and wet) performed in the precooler, the cycle mechanisms are explained as follows. The exhaust flow exiting the combustor (sCO_2 and water vapor) at high pressure (200–300 bar) and temperature (550–750 °C) (state 1) is expanded through the GT to low pressure (75–116 bar) and temperature above 370 °C (state 2). Then, the exhaust flow enters the HTR (2–3) and LTR (3–4) to transfer heat from the hot exhaust flow to the recycled sCO_2 stream (7–11). Exiting the recuperators, the exhaust flow is cooled in the precooler (4–5) and the combustion derived water is separated through the water separator (5–6). To maintain mass balance within the cycle, with a pressure drop of 5% (justified in section 3.3) through the recuperators, precooler, and water separator, part of the high purity sCO_2 flow is exported at sufficient pressure (75–110 bar) for CO_2 pipelines used in CO_2 sequestration or commercial utilization (6). The other part is compressed in the GC (6–7) and heated by the LTR (7–10) and HTR (10–11) before entering the oxy-combustor. With the presence of the recycled sCO_2, a pressurized fuel (13) is mixed with compressed oxygen (16), which is generated by an air
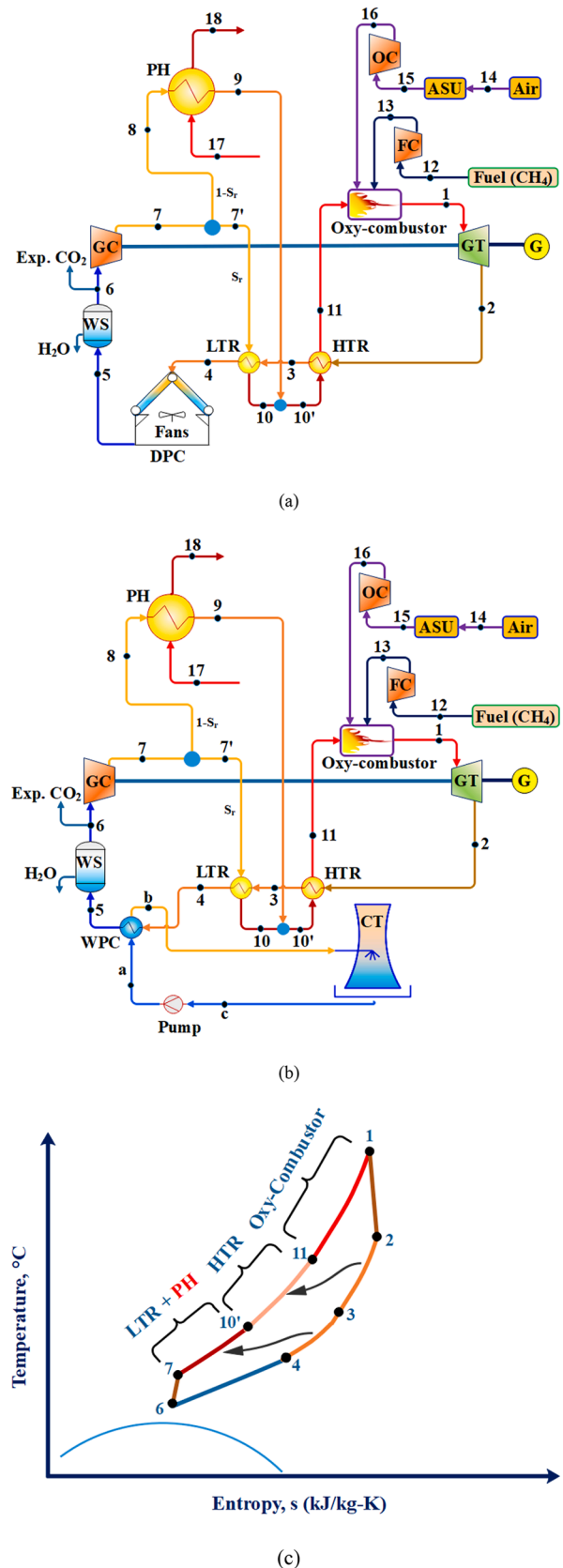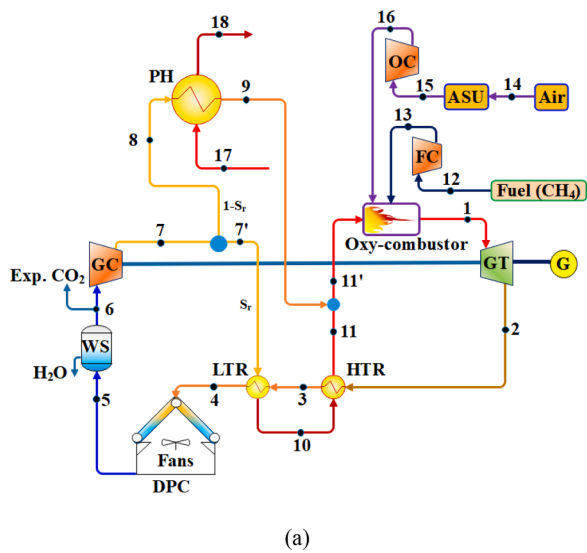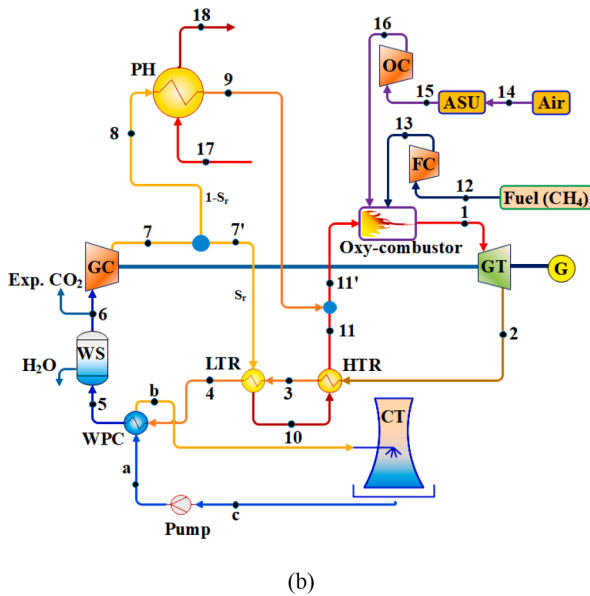

(a)

(b)

(c)

Fig. 2. Layout configuration (M2) of the direct oxy-combustor cycle with (a) dry-cooling, (b) wet-cooling processes with a preheater connected in parallel with the LTR, and (c) T-s diagram.
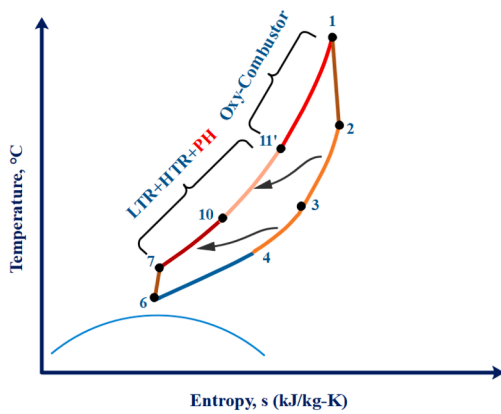
(a)

(b)

(c)

Fig. 3. Layout configuration (M3) of the direct oxy-combustor cycle with (a) dry-cooling, (b) wet-cooling processes with a preheater connected in parallel with both HTR and LTR, and c) T-s diagram.
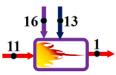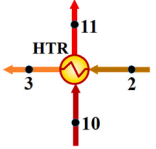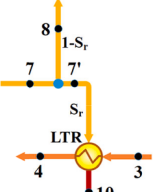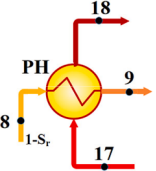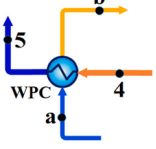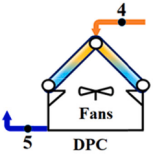
separation unit (ASU), and combusted in the oxy-combustor. The exhaust flow is directed to the inlet of the turbine to repeat the cycle.

The wet-cooling method (wet-cooling tower, as shown in Fig. 1(b)) was used in various direct oxy-combustor sCO_2 power cycles to cool the exhaust flow to a low temperature (between 15 °C and 33 °C). On the others side, the dry-cooling method (air cooler) was mostly used in indirect sCO_2 power cycles to cool the sCO_2 to a temperature between 40 °C and 50 °C [44,45]. From a thermodynamic point of view, the wet-cooling method characteristics including the high cooling capacity, and high reliability in hot climate conditions make it the best choice especially for large cooling demand [42]. However, from an economic point of view, the dry-cooling method has lower capital and maintenance costs and exhibits the ability to work in different climate conditions (from hot to humid and extremely cold conditions). Sleiti et al. [40] have investigated the thermodynamic and exergoeconomic performances of the oxy-combustion sCO_2 power cycle under dry-cooling conditions. However, it is not clear which is better (dry or wet-cooling) in terms of optimized levelized cost of electricity (LCOE) and other PIs of the cycle. Therefore, the present study introduces a comprehensive investigation and comparison between the wet-cooling and dry-cooling methods for the M1 cycle configuration shown in Fig. 1 as well as for M2 and M3 configurations shown in Fig. 2, and Fig. 3, respectively.

In M1 (Fig. 1), due to the lower specific heat of the exhaust flow in the hot side of the recuperators compared to that of the recycled sCO_2 in the cold side, there is not enough heat to raise the temperature of the recycled sCO_2 to an acceptable level. Thus, a significant imbalance is noted between the heat rejected by the recuperators (2–4) and the heat required to raise the temperature of the recycled sCO_2 (7–11). The imbalance can be corrected by adding heat from the adiabatic operation of the ASU air compressors and the CO_2 recycle compressor [24]. However, this arrangement will increase the specific energy consumption of the ASU and reduce the operational flexibility of the system [27]. In addition, the internal heat recovery from the ASU dictates an extremely large heat transfer area for the recuperators as it has to transfer about 2.9 MW per MW of net electrical power [21]. This increases the design complexity and the capital cost of the recuperators. Alternatively, the present study proposes a viable solution for this issue by integrating a preheater to be connected in parallel with the LTR as shown in M2 cycle configuration (Fig. 2) and in parallel with both LTR and HTR as shown in M3 cycle configuration (Fig. 3).
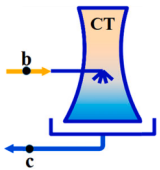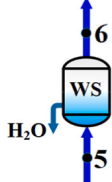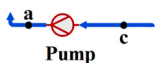
Referring to Fig. 2 and Fig. 3, the mechanism of the preheating process is explained next. The recycled sCO_2 flow is split at the outlet of the GC (state 7) into two streams. One stream is to pass through the LTR ((7′-10) in M2) and in both LTR and HTR ((7′-11) in M3) while the other stream is to pass through the preheater (8–9). This way, the mass flow rate through the recuperator is adjusted to correct the aforementioned imbalance and the pinch-point problem [40,46,47] is eliminated. Another advantage of the preheating processes of M1 and M2 configurations is that the preheater could be driven by a wide variety of waste heat sources with a temperature range of 300–600 °C [48] (at the preheating fluid inlet (state 17)), which enhances the temperature of the recycled sCO_2 at the inlet of the combustor (state 11). This minimizes the consumed fuel in the combustor although it adds additional cost for the preheater. Thus, it is important to assess the effect of integrating a preheater in terms of the overall thermal efficiency and LCOE as investigated and discussed in detail in this study. Moreover, it was found that configuration M2 is suitable with waste heat sources inlet temperature (T_{17}) less than 400°C, while configuration M3 is more suitable for higher temperatures. In the present study, the proposed configurations (M1, M2, and M3) are investigated for turbine inlet temperature range between 550 and 750 °C. This eliminates the need to cool the gas turbine (which is performed in the Allam cycle) and simplifies the design of the recuperators.

Table 1

Energy and exergy equations of the layout components.

Component	Model	Equations
Gas turbine		$\dot{m}_1 = \dot{m}_2 = \dot{m}_{CO_2} + \dot{m}_{H_2O}$ $\dot{W}_{GT} = \eta_t \times \dot{m}_1(h_1 - h_{2s}) \dot{E}_{F,GT} = \dot{m}_1(\varphi_1 - \varphi_2)$ $\dot{E}_{P,GT} = \dot{W}_{GT}$ $\eta_{GT} = \dfrac{h_1 - h_2}{h_1 - h_{2s}}, \varepsilon_{GT} = \dfrac{\dot{E}_{P,GT}}{\dot{E}_{F,GT}}$
Gas compressor		$\dot{m}_6 = \dot{m}_7 = \dot{m}_{rCO_2}$ $\dot{W}_{GC} = \dot{m}_6(h_{7s} - h_6)/\eta_{GC} \dot{E}_{F,GC} = \dot{W}_{GC} \dot{E}_{P,GC} = \dot{m}_7(\varphi_7 - \varphi_6)_{CO_2}$ $\eta_{GC} = \dfrac{h_{7s} - h_6}{h_7 - h_6}, \varepsilon_{GC} = \dfrac{\dot{E}_{P,GC}}{\dot{E}_{F,GC}}$
Direct oxy-combustor		$\dot{m}_1 = \dot{m}_{11} + \dot{m}_{16} + \dot{m}_{13}$ $\dot{m}_{11} = \dot{m}_{rCO_2}, \dot{m}_{16} = \dot{m}_{O_2}, \dot{m}_{13} = \dot{m}_f$ $\dot{Q}_{oc} = \dot{m}_1 h_1 - \dot{m}_{16} h_{16} - \dot{m}_{13} h_{13} - \dot{m}_{11} h_{11}$ $\dot{Q}_{oc} = \dot{m}_f \cdot \mathrm{LHV} E_{F,oc} = \dot{E}_{11} + \dot{E}_{13} + \dot{E}_{16} \dot{E}_{P,t} = \dot{E}_1$ $\varepsilon_{oc} = \dfrac{\dot{E}_{P,oc}}{\dot{E}_{F,oc}}$
HTR		$\dot{m}_2 = \dot{m}_3 = \dot{m}_{CO_2} + \dot{m}_{H_2O}$ $\dot{m}_{10} = \dot{m}_{11} = \dot{m}_2 = \dot{m}_{rCO_2}$ (in M1 & M2) $\dot{m}_{11} = S_r \dot{m}_{rCO_2}$ (in M3) $\dot{Q}_{HTR} = \dot{m}_2(h_2 - h_3) = \dot{m}_{11}(h_{11} - h_{10})$ $\dot{E}_{F,HTR} = \dot{E}_2 - \dot{E}_3$ $\dot{E}_{P,HTR} = \dot{E}_{11} - \dot{E}_{10}$ $\varepsilon_{HTR} = \dfrac{\dot{E}_{P,HTR}}{\dot{E}_{F,HTR}}$
LTR		$\dot{m}_3 = \dot{m}_4 = \dot{m}_{CO_2} + \dot{m}_{H_2O}$ $\dot{m}_7 = \dot{m}_{7\acute{A}} = \dot{m}_{10} = \dot{m}_{rCO_2}$ (in M1) $\dot{m}_{7\acute{A}} = \dot{m}_{10} = S_r \dot{m}_7$ (in M2 & M3) $\dot{Q}_{LTR} = \dot{m}_3(h_3 - h_4) = \dot{m}_{7\acute{A}}(h_{10} - h_{7\acute{A}})$ $\dot{E}_{F,LTR} = \dot{E}_3 - \dot{E}_4$ $\dot{E}_{P,LTR} = \dot{E}_{10} - \dot{E}_{7\acute{A}}$ $\varepsilon_{LTR} = \dfrac{\dot{E}_{P,LTR}}{\dot{E}_{F,LTR}}$
Preheater		$\dot{m}_{17} = \dot{m}_{18} = \dot{m}_{ph}$ $\dot{m}_9 = \dot{m}_8 = S_r \dot{m}_7$ (in M2 & M3) $\dot{Q}_{PH} = \dot{m}_{ph}(h_{17} - h_{18}) = \dot{m}_9(h_9 - h_8)$ $\dot{E}_{F,PH} = \dot{E}_{17} - \dot{E}_{18}$ $\dot{E}_{P,PH} = \dot{E}_9 - \dot{E}_8$ $\varepsilon_{PH} = \dfrac{\dot{E}_{P,LTR}}{\dot{E}_{F,LTR}}$
Wet precooler (Water cooler)		$\dot{m}_4 = \dot{m}_5 = \dot{m}_{CO_2} + \dot{m}_{H_2O}$ $\dot{m}_a = \dot{m}_b = \dot{m}_{cw}$ $\dot{Q}_{WPC} = \dot{m}_4(h_4 - h_5) = \dot{m}_{cw}(h_b - h_a)$ $\dot{E}_{F,WPC} = \dot{E}_4$ $\dot{E}_{P,WPC} = \dot{E}_5$ $\dot{E}_{L,WPC} = \dot{E}_b - \dot{E}_a$ $\varepsilon_{WPC} = \dfrac{\dot{E}_{P,WPC}}{\dot{E}_{F,WPC}}$
Dry precooler (Air cooler)		$\dot{m}_4 = \dot{m}_5 = \dot{m}_{CO_2} + \dot{m}_{H_2O}$ $\dot{Q}_{DPC} = \dot{m}_4(h_4 - h_5)$ $\dot{E}_{F,DPC} = \dot{E}_4$ $\dot{E}_{P,DPC} = \dot{E}_5$ $\dot{E}_{L,DPC} = \dot{E}_{a,in} - \dot{E}_{a,out}$ $\varepsilon_{WPC} = \dfrac{\dot{E}_{P,DPC}}{\dot{E}_{F,DPC}}$

Table 1 (*continued*)

Component	Model	Equations
Cooling tower		$\dot{m}_b = \dot{m}_c = \dot{m}_{cw}$ $\dot{Q}_{CT} = \dot{m}_{cw}(h_b - h_c)$
Water separator		$\dot{m}_5 = \dot{m}_{CO_2} + \dot{m}_{H_2O}$ $\dot{m}_6 = \dot{m}_{rCO_2}$
Pump		$\dot{m}_c = \dot{m}_a = \dot{m}_{cw}$ $\dot{W}_{pump} = \dot{m}_{cw}(h_a - h_c)/\eta_{pump}$
Fuel compressor		$\dot{m}_{12} = \dot{m}_{13} = \dot{m}_f$ $\dot{W}_{FC} = \dot{m}_{12}(h_{13s} - h_{12})/\eta_{FC} \dot{E}_{F,FC} = \dot{W}_{FC}$ $\dot{E}_{P,FC} = \dot{m}_{12}(\varphi_{13} - \varphi_{12})$ $\eta_{FC} = \dfrac{h_{13s} - h_{12}}{h_{13} - h_{12}}, \varepsilon_{FC} = \dfrac{\dot{E}_{P,FC}}{\dot{E}_{F,FC}}$
Oxygen compressor		$\dot{m}_{15} = \dot{m}_{16} = \dot{m}_{O_2}$ $\dot{W}_{OC} = \dot{m}_{15}(h_{16s} - h_{15})/\eta_{OC} \dot{E}_{F,OC} = \dot{W}_{OC}$ $\dot{E}_{P,OC} = \dot{m}_{15}(\varphi_{16} - \varphi_{15})$ $\eta_{OC} = \dfrac{h_{16s} - h_{15}}{h_{16} - h_{15}}, \varepsilon_{OC} = \dfrac{\dot{E}_{P,OC}}{\dot{E}_{F,OC}}$

3. Thermodynamic and thermoeconomic modeling

The performance of the proposed configurations is evaluated from both thermodynamic and economic viewpoints. Section 3.1 presents the thermodynamic energy and exergy models of each component of the studied layouts. The LCOE is calculated based on a detailed model which is presented in section 3.2. The solution procedures and the design values (range) of the model parameters are explained in section 3.3. Then, the results of the developed model are validated in section 3.4.

3.1. Energy and exergy modeling

The thermodynamic model of each layout component along with the exergy model is derived in terms of the mass, energy, and exergy balance equations, respectively [49]:

$$\sum \dot{m}_i = \sum \dot{m}_o \tag{1}$$

$$\sum \dot{Q} + \sum \dot{m}_i h_i = \sum \dot{W} + \sum \dot{m}_o h_o \tag{2}$$

$$\dot{E}_Q + \sum \dot{E}_i = \dot{E}_W + \sum \dot{E}_o + \dot{E}_D \tag{3}$$

The details of how Eqs. 1–3 are applied to each component of the sCO$_2$ power cycles are presented in
Table 1. Neglecting the changes of the kinetic and potential exergies, the exergy of each stream is expressed as the sum of the physical and chemical exergies:

$$\dot{E} = \dot{E}_{ph} + \dot{E}_{ch} \tag{4}$$

The physical end chemical exergies are given as [50]:

$$\dot{E}_{ph} = \dot{m}\varphi \tag{5}$$

$$\varphi = (h - h_o) - T_o(s - s_o) \tag{6}$$

$$\dot{E}_{ch} = \dot{n}\left[\sum_{j=1}^{n} x_j e_j^o + RT_o \sum_{j=1}^{n} x_j \ln(x_j)\right] \tag{7}$$

where $\dot{n}$ is the molar flow rate, x_j is the molar fraction of jth component in a mixture, and e_j^o is the standard chemical exergy of jth component at T_o and P_o conditions. In this study, the fuel-product-loss method is used to evaluate the exergy efficiency of each layout component and the overall exergy efficiency of each configuration. For kth component, the balanced equation of fuel-product-loss exergies and its exergy efficiency are given in Eq. (8) and Eq. (9), respectively [51,52].

$$\dot{E}_{D,k} = \dot{E}_{F,k} - \dot{E}_{P,k} - \dot{E}_{L,k} \tag{8}$$

$$\varepsilon_k = \frac{\dot{E}_{P,k}}{\dot{E}_{F,k}} \tag{9}$$

The heat exchangers (LTR, HTR, preheater, and precooler) were modeled based on the effectiveness method using Eq. (10) [53]. To take the dramatic change of the specific heat of the CO$_2$ with temperature variation, each heat exchanger is discretized into sub-heat exchangers with equal lengths.

$$\in = \frac{\dot{Q}}{\dot{Q}_{max}} \tag{10}$$

To complete the thermodynamic model, it is necessary to relate the mass flow rate of the oxygen and recycled sCO$_2$ with the mass flow rate

Table 2

Cost correlations of the layout components baselined to 2019 U.S. dollars using the average Chemical Engineering Plant Cost Index (CEPCI) for 2019 (the last full year for which CEPCI values were available for this study) [55].*

Component	Component cost	Installation cost	
		Materials**	Direct labor**
Oxy-combustor	$Z_{oc} = 677203 \times \dot{Q}_{oc}^{0.6} \times f_{T,oc}$ $f_{T,oc} = 1 + 5.4 \times 10^{-5}(T_{max} - 550)^2$	8%	12%
Gas turbine	$Z_{GT} = 195382 \times \dot{W}_{GT}^{0.5561} \times f_{T,GT}$ $f_{T,GT} = 1 + 1.106 \times 10^{-4}(T_{max} - 550)^2$	8%	12%
Generator	$Z_{G} = 116577 \times \dot{W}_{net}^{0.5463}$	8%	12%
Gearbox	$Z_{GB} = 189693 \times \dot{W}_{GT}^{0.2434}$	8%	12%
Compressor	$Z_{GC} = 1316100 \times \dot{W}_{C}^{0.3992}$	8%	12%
HTR	$Z_{HTR} = 52.91 \times (UA)_{HTR}^{0.7544} \times f_{T,HTR}$ $f_{T,HTR} = 1 + 0.02141(T_{max} - 550)$	2%	3%
LTR	$Z_{LTR} = 52.91 \times (UA)_{LTR}^{0.7544} \times f_{T,LTR}$ $f_{T,LTR} = 1 + 0.02141(T_{max} - 550)$	2%	3%
Preheater	$Z_{PH} = 52.91 \times (UA)_{ph}^{0.7544} \times f_{T,PH}$ $f_{T,PH} = 1 + 0.02141(T_{max} - 550)$	2%	3%
Dry-Precooler	$Z_{DPC} = 35.18 \times (UA)_{DPC}^{0.75}$	8%	12%
Wet-Precooler	$Z_{WPC} = 52.91 \times (UA)_{WPC}^{0.7544} \times f_{T,WPC}$ $f_{T,WPC} = 1 + 0.02141(T_{max} - 550)$	2%	3%
Pump [56]	$Z_{pump} = 10.51^3 \times (\frac{\dot{W}_{pump}}{4})^{0.55} \times$	2.5	2.5
Cooling tower [57]	$Z_{CT} = 24.17 \times \dot{Q}_{WPC} + 2060.28$	2.5	2.5
ASU [58]	$Z_{ASU} = RefCost \times (Size/RefSize) \times OIF$, $RefCost = 151 MillionUS\$(2019)$, $Size = \dot{m}_{O_2}$, $RefSize = 52 kgO_2/s, OIF = 1$	8%	12%

*$\dot{W}_{GT}$, $\dot{W}_{net}$, $\dot{W}_{C}$, and Q_{oc} are in MW, (UA) in W/°C, $\dot{Q}_{WPC}$, and $\dot{W}_{pump}$ in kW.
**As a percentage of the component cost.

of the fuel (assumed to be pure methane (CH_4)) and the mass flow rate of the CO_2 at the exit of the combustor:

$$\dot{m}_{O_2} = 4\dot{m}_f \tag{11}$$

$$\dot{m}_{rCO_2} = \dot{m}_{CO_2} - 2.75\dot{m}_f \tag{12}$$

Equations 11–12 were derived from the chemical equation of the actual combustion in the reactor, which is given as:

$$CH_4 + CO_2 + 2O_2 \rightarrow 2CO_2 + 2H_2O \tag{13}$$

From Eq. (13), it can be noted that 2 kmol of oxygen is needed for each kmol of the fuel. The molar weight of the oxygen is 32 kg/kmol and the molar weight of the fuel (CH_4) is 16 kg/kmol. Therefore, for each 16 kg of fuel, 64 kg of oxygen is needed. Mathematically, the mass flow rate of the oxygen equals 4 times the mass flow rate of the fuel as shown in Eq. (11). For ideal combustion (without recycled CO_2), 1 kmol of the carbon dioxide (CO_2) is produced for each kmol of the combusted fuel. As the molecular weight of CO_2 is 44 kg/kmol, then each 16 kg of the fuel produces 44 kg of CO_2, which is 2.75 higher than the mass of the fuel. Thus, the recycled CO_2 is equal to the total CO_2 at the outlet of the combustor minus the newly produced CO_2 in the combustor ($\dot{m}_{new,CO_2} =$

2.75$\dot{m}_f$) as expressed in Eq. (12).

For the overall system and to conclude the effect of the preheater on the minimization of the consumed fuel, the thermal efficiency η_{th} is defined without including the preheating load as follows:

$$\eta_{th} = \frac{\dot{W}_{net}}{\dot{m}_f \times LHV} \tag{14}$$

where $\dot{W}_{net}$ is the net output power of the system and calculated as:

$$\dot{W}_{net} = \eta_g(\dot{W}_{GT} - \dot{W}_{GC} - \dot{W}_{FC} - \dot{W}_{OC} - \dot{W}_{pump} - \dot{W}_{ASU}) \tag{15}$$

To take the preheater load into account, the overall efficiency $\eta_{th,overall}$ of the cycle is given as:

$$\eta_{th,overall} = \frac{\dot{W}_{net}}{\dot{Q}_{PH} + \dot{m}_f \times LHV} \tag{16}$$

The overall exergy of the cycle is given as:

$$\varepsilon_o = \frac{\sum \dot{E}_{P,k}}{\sum \dot{E}_{F,k}} \tag{17}$$

3.2. Thermoeconomic modeling

The economic evaluation of the proposed configurations is performed in terms of the LCOE which is calculated according to Eq. (18) [54].

$$LCOE = \frac{PC - PV_{DTS} + PV_{LOC} - PV_{SC}}{LEP} \tag{18}$$

where *PC* is the project cost, which is the sum of the components and installation costs (given in Eq. (19)), PV_{DTS} is the present value of the depreciation tax shield (given in Eq. (20)), PV_{LOC} is the present value of lifetime operating costs (given in Eq. (21)), PV_{SC} is the present value of salvage costs (assumed $0.00), and *LEP* is the lifetime electrical production (given in Eq. (22)).

$$PC = \sum (Component cost + Installation cost)_k \tag{19}$$

$$PV_{DTS} = TR \times PC/(1 + DR)^{DP} \tag{20}$$

$$PV_{LOC} = n^*(OMC + Cost of the fuel)/(1 + DR)^n \tag{21}$$

$$LEP = PUF \times n \times \dot{W}_{net} \times 8760 \tag{22}$$

where *TR* is the tax rate (35%), [54], *DR* is the discount rate (2%), *DP* is the depreciation period (10 years), *n* is the lifetime of the plant (20 years), and *PUF* is the plant utilization factor (85%). Table 2 presents the components' cost functions and the installation costs for the component materials and direct labor, which were calculated as a percentage of the component costs [55].

3.3. Solution procedures

Table 3 shows the input parameters for the analysis of the proposed configurations in this study including the cycle parameters, pressure drops through components, specifications of the waste heat source used in the preheater, and the parameters of the economic evaluation. Thorough energy, exergy, and economic model for each configuration are coded and solved in the engineering equation solver (EES) software and the thermodynamic properties at each state were obtained from its library. The state points (temperature, pressure, mass flow rate, enthalpy, and entropy) of M1, M2, and M3 at the design point parameters of wet and dry cooling conditions are presented in Table A. 1 (Appendix A). Then, single- and multi-objective optimization are performed using a genetic algorithm (GA). GA method was chosen among several other optimization methods because of its robustness and is not

Table 3
Input parameters of the direct oxy-fuel preheated sCO$_2$ cycle.

	Parameter	Range/Design value
Cycle parameters	Higher pressure, P_h (bar)	200–300
	Lower pressure, P_l (bar)	75–100
	Maximum cycle temperature, T_{max} (°C)	550–750
	Compressor inlet temperature, T_{min} (°C)	50 (Dry), 32 (Wet)
	Split ratio, S_r	0.2–0.8
	Net electrical power, $\dot{W}_{net}$ (MW)	50–100
	Efficiency of the generator, η_g (%)	95
	Efficiency of the gas turbine, η_{GT} (%)	90
	Efficiency of the gas compressors, η_{GC} (%)	85
	LHV-methane, (kJ/kg)	50,050
	Power consumed by the air separation unit, (%) [61]	20
Pressure drops	Combustor, (%) [62]	3
	Recuperators (high pressure side), (%) [21]	1
	Recuperators (low pressure side), (%) [62]	3
	Precooler and water separator, (%) [21]	2
Preheater	Inlet temperature of the preheater fluid, T_{17} (°C) [63,64]	370 (for M2), 540 (for M3)
	Mass flow rate of the preheater fluid, $\dot{m}_{ph}$ [63,64]	89 (for M2), 178 (for M3)
	Minimum pinch point of the preheater, (°C)	10
	Preheating fluid (assumed)	Air
Economic parameters	Plant lifetime, (years)	20
	Depreciation period, DP (years)	10
	Tax rate, (%)	35
	Plant utilization factor, PUF (%)	85
	Cost of the fuel, ($/kWh$_e$)	0.07
	Operating and maintenance cost, ($/kWh$_e$)	0.008

affected by the guessed initial values like the other methods [59,60].

3.4. Validation

The validation of the developed model of the proposed configurations is conducted by comparing the results to those reported by the original developers of Allam cycle [24]. Also, the model is validated against results obtained by the model developed by Scaccabarozzi et al. [21]. In both cases, the major operating conditions were adjusted to be the same as in Ref. [24] and Ref. [21] under the same net electrical output power. The validation results are summarized in Table 4. From Table 4, it can be noted that the maximum residual error compared to Allam et al. [24] data is −3.90% in the thermal energy of the fuel. This returns to that this study treats the natural gas as pure methane, which yields a difference in the released heat from the combusted fuel.

Comparing to Scaccabarozzi et al. [21], a maximum error of 3.85% associated with the turbine outlet temperature is observed. The is attributed mainly to the slight difference in the composition of the exhaust flow from the combustor between the present study and Scaccabarozzi et al. [21]. In both data sets, the error of the net electric efficiency does not exceed 1%, which is sufficient for the validation of the proposed model.

At $T_1 = 1150$ °C, $T_6 = 26$ °C, $P_1 =$,300 bar and $P_6 = 32.2$ bar.

4. Results and discussion

In this section, the results of the energy, exergy, and economic analyses are presented and discussed. Parametric studies are carried out for the major operating conditions including the split ratio, maximum and minimum cycle temperatures, pressures, and waste heat source specifications (sections 4.1–4.5). Then, single- and multi-objective optimizations are performed (section 4.6) for the proposed configurations by considering thermal efficiency, exergy efficiency, and LCOE as objective functions using a genetic algorithm method.

4.1. Split ratio effect

Split ratio (S_r) refers to the ratio of the recycled sCO$_2$ flow portion that passes through the LTR (in M2) and both LTR and HTR (in M3) to the total recycled flow at the exit of the GC. Fig. 4 shows the variation of the (a) thermal efficiency, (b) overall thermal efficiency, (c) exergy efficiency, and (d) LCOE with S_r for both wet and dry-cooling conditions.

As mentioned above, the thermal efficiency was defined relative to the heat released in the combustor (without including the preheater load) to evaluate the effect of the preheater in the minimization of the consumed fuel. As shown in Fig. 4(a), the increase of S_r slightly decreases the thermal efficiency for all cases except for M2 and M3 in wet-cooling conditions. In wet-cooling conditions for M2 and M3, a significant decrease in the thermal efficiency of 2.3% and 3.97%, respectively, is observed for S_r higher than 0.73. In contrast to the thermal efficiency behavior, the exergy efficiency (Fig. 4(c)) increases with S_r up to 0.73 then stabilizes or slightly decreases for S_r higher than 0.73. This is because the increase of S_r increases the load of the LTR and HTR (in M2 and M3 configurations), which minimizes the temperature at the combustor inlet (T_{17}) and increases the fuel consumption in the combustor. At the same time, the increase of S_r reduces the temperature at the inlet of the precooler, which significantly reduces the exergy destruction rate and improves the exergy efficiency of the system. Therefore, $S_r = 0.73$ is considered an optimum value and is used as the design value for the parametric analyses of the other operating conditions.

For all configurations, it can be noted that the thermal efficiency of M3 is higher than that of M2 (by 5.81% (wet), and 3.27% (dry)) and M1 (by 13.27% (wet), and 6.58% (dry)). This confirms that the integration of the preheater minimizes the fuel consumption in the combustor. For instance, at the design point conditions, the mass flue rates of the fuel

Table 4
Validation results of the proposed model compared to results published in the literature.

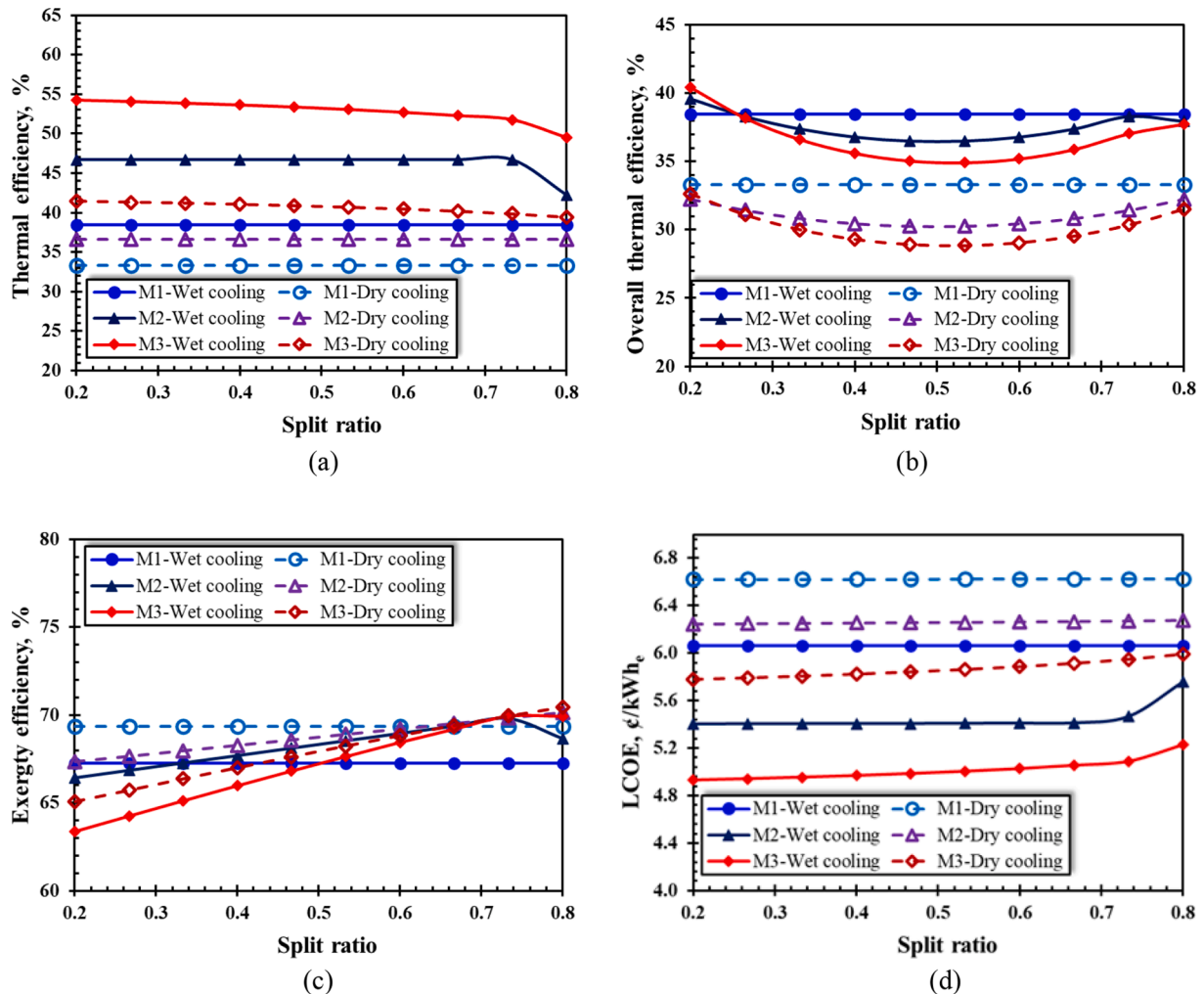| Items	Allam et al. [24]	Present work	Error (%)	Scaccabarozzi et al. [21]	Present work	Error (%)
Net electrical power output (MW$_e$)	303	303	0.00	419.31	419.31	0.00
Thermal energy of the fuel (LHV) (MW$_{th}$)	511	531	−3.90	768.31	775.20	−0.89
Turbine power output (MW)	–	453.8	–	622.42	637.20	−2.37
Recycle flow compression (MW)	77.00	78.40	–	111.15	112.86	−1.54
NG compressor consumption (MW)	–	2.80	–	4.18	4.32	−3.35
ASU penalty (MW)	56.00	58.80	−1.82	85.54	83.86	1.90
Turbine outlet temperature (°C)	727.0	738.5	−1.6	741.2	769.6	−3.83
Recycle flow final temperature (°C)	–	762.0	–	721.2	734.8	−1.89
Turbine inlet flow rate	923	914.6	0.91	1271	1268	0.24
Total recycle flow rate (with oxygen) (kg/s)	881.0	890.0	−1.02	1353.9	1353.5	0.03
Net electrical efficiency (%)	59.30	58.84	0.78	54.58	54.09	0.90

Fig. 4. Maximum cycle pressure effect on (a) thermal efficiency, (b) overall thermal efficiency, (c) exergy efficiency, and d) LCOE at wet and dry-cooling conditions.

are 2.70 kg/s in M1, 2.25 kg/s in M2, and 2.00 kg/s in M3 (for wet-cooling) and 3.11 kg/s in M1, 2.83 kg/s in M2, and 2.59 kg/s in M3 (for dry-cooling). However, when the preheating load is included, the overall thermal efficiency (Fig. 4(b)) of M1 is higher than M2 and M3 at S_r higher than 0.23. However, low S_r values require a large load on the preheater, which is not acceptable from a practical point of view, since the achievable preheating load depends on the characteristics of the heat source. Regarding the effect of the wet and dry-cooling conditions, it can be noted that the wet-cooling significantly improves both the thermal and the overall thermal efficiencies, which accordingly minimizes the LCOE as shown in Fig. 4(d). However, the exergy efficiency of the dry-cooling configurations is higher than in wet-cooling conditions. This returns to that the temperature differences become larger in the recuperator with the wet-cooling method.

An interesting result is noted that the thermal efficiency of M3 in dry-cooling conditions is higher than M1 in wet-cooling conditions by 1.5%, as shown in Fig. 4(a). This implies that the improvement achieved by the preheater in M3 (by minimizing consumed fuel) is more than the improvement achieved by the wet-cooling in M1 (by minimizing the compression power). This also makes the LCOE in M3 (dry-cooling) lower than of M1 (wet-cooling) by 2.4% over the range of S_r.

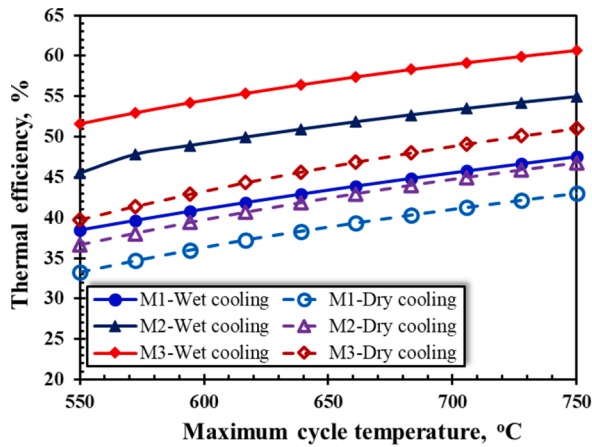### 4.2. Effect of the maximum cycle temperature

Fig. 5 shows the effect of the maximum cycle temperature T_{max} (at the turbine inlet) on the (a) thermal efficiency, (b) overall thermal
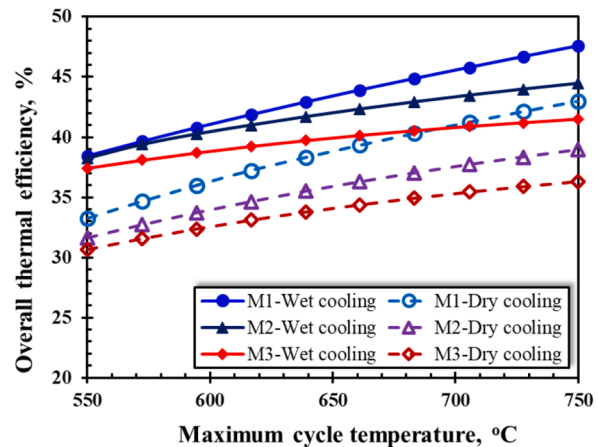
efficiency, (c) exergy efficiency, and (d) LCOE of the proposed configurations for both wet and dry-cooling conditions.

It can be noted from Fig. 5(a) that the increase of T_{max} from 550 °C to 750 °C improves the thermal efficiency by 8.3% (at least) for all cases. Also, the overall thermal efficiency is improved by 4.1% (at least) for all cases, as shown in Fig. 5(b). However, the overall efficiencies of M1 and M2 (wet) at $T_{max} \leq 594$ °C are almost the same. This is because the reduction of the fuel consumption in M2 ($T_{max} \leq 594$ °C) is equivalent to the heat supplied by the preheater, which yields overall efficiency similar to that of M1. This implies that the integration of the preheater significantly improves the thermal efficiency of M2 compared to M1 (by 8%) with a slight decrease in the overall thermal efficiency (less than 0.87%). Furthermore, at $T_{max} \leq 594$ °C (wet), the increase of the recycled sCO$_2$ temperature at the inlet of the combustor in M3 is only 14 °C higher than in M2, which reduces the fuel consumption by 0.23 kg/s. This slightly affects the economic performance of M3 compared to M2 and their LCOE is almost the same (at $T_{max} \leq 594$ °C) and less than of M1 as shown in Fig. 5(d).

Therefore, M2 configuration can be recommended for wet-cooling conditions at turbine inlet temperatures less than 594 °C and waste heat source temperatures less than 400 °C (which is used for M2 configuration). From Fig. 5(b), it can be noted that the overall efficiency of M1 (dry) is higher than that of M3 (wet) at $T_{max} > 683$ °C. However, the thermal efficiency of M3 (wet) is about 1.5 times higher than that of M1 (dry). Thus, as noted for all scenarios, the LCOE of wet-cooling configurations is much lower than of dry-cooling conditions (by 21%).
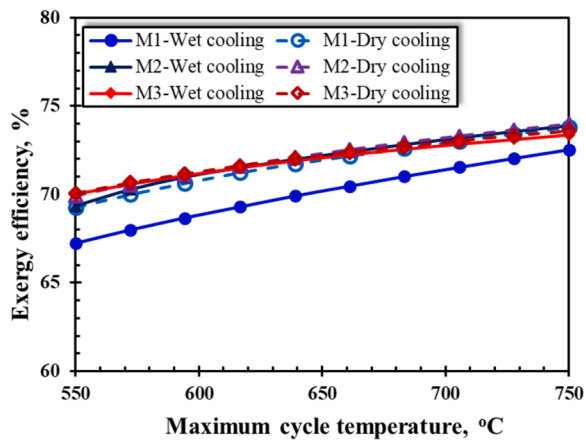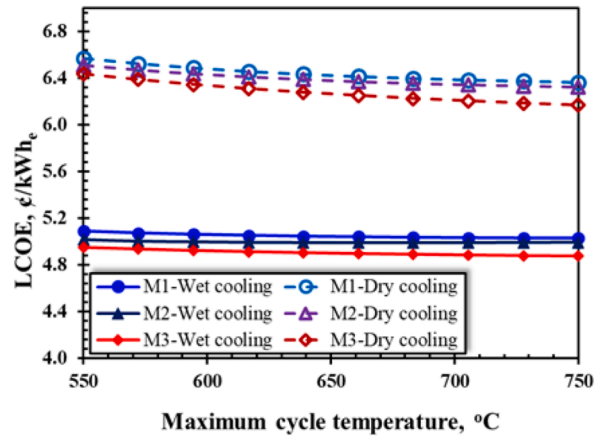
Fig. 5. Maximum cycle temperature effect on (a) thermal efficiency, (b) overall thermal efficiency, (c) exergy efficiency, and (d) LCOE at wet and dry-cooling conditions.

The significant difference between the results of the wet and dry cooling conditions returns to several reasons including that the wet-cooling method:

Fig. 6. Effect of the power plant capacity on LCOE at wet and dry-cooling conditions.

- reduces the compression power consumed by the GC by about 45% compared to that consumed in dry conditions. For instance, at the design point of the proposed cycles, the compression power is 17.88 MW in wet cooling compared to 32.21 MW in dry cooling. This is because in wet conditions, the sCO_2 behaves as a liquid-like fluid, which minimized the compression power and the size of the GC.
- minimizes the temperature levels at the terminals of the recuperators and increases the temperature differences between the hot and cold streams, which minimizes the required heat transfer area and thus the LCOE. In wet cooling, at the design point, the outlet temperature from the GC (state 7) is 99 °C compared to 153 °C in dry conditions. Therefore, the heat recovered in wet conditions is higher than in dry conditions with more compact size of the heat exchangers.
- reduces the cooling load of the precooler (by 10%) compared to the dry method. For instance, at the design point, the precooler loads for M1, M2, and M3 are 69.7 MW, 85.1 MW, and 102.2 MW in wet cooling, respectively, compared to 77.1 MW, 96.7 MW, and 113.1 MW in dry cooling, respectively. This is because the higher outlet temperature from the GC in dry cooling limits the heat recovered from the LTR and increases the temperature at the inlet of the precooler.

Fig. 6 shows the effect of the power plant capacity ($\dot{W}_{net}$) on the LCOE of the proposed configurations in wet and dry-cooling conditions at T_{max} of 650 °C. For both wet and dry scenarios, the increase of

(a)

(b)

(c)

(d)

(e)

(f)
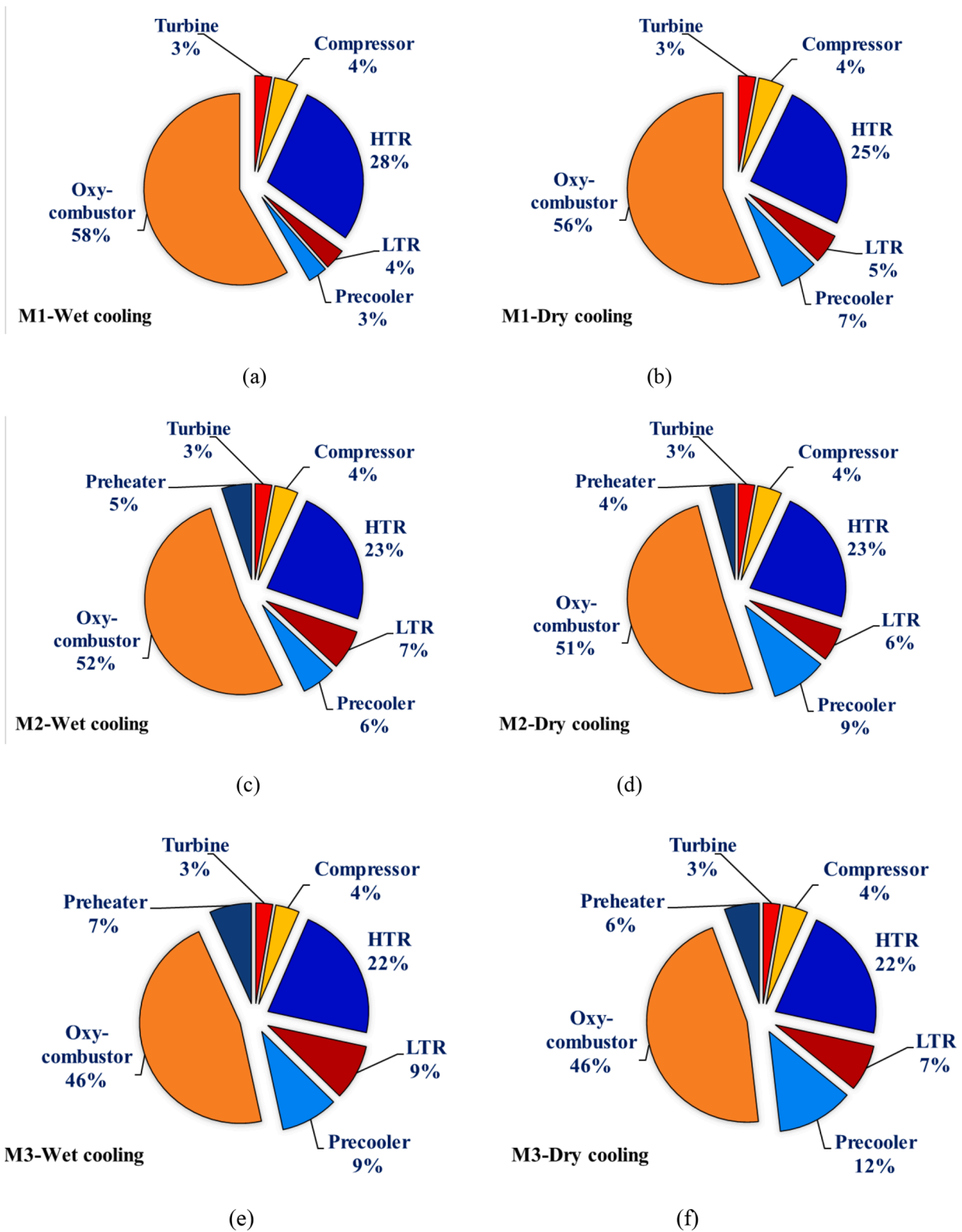
Fig. 7. Exergy destruction for each component of the proposed configurations in wet and dry-cooling conditions at $S_r = 0.73$ and $T_{max} = 750$ °C.
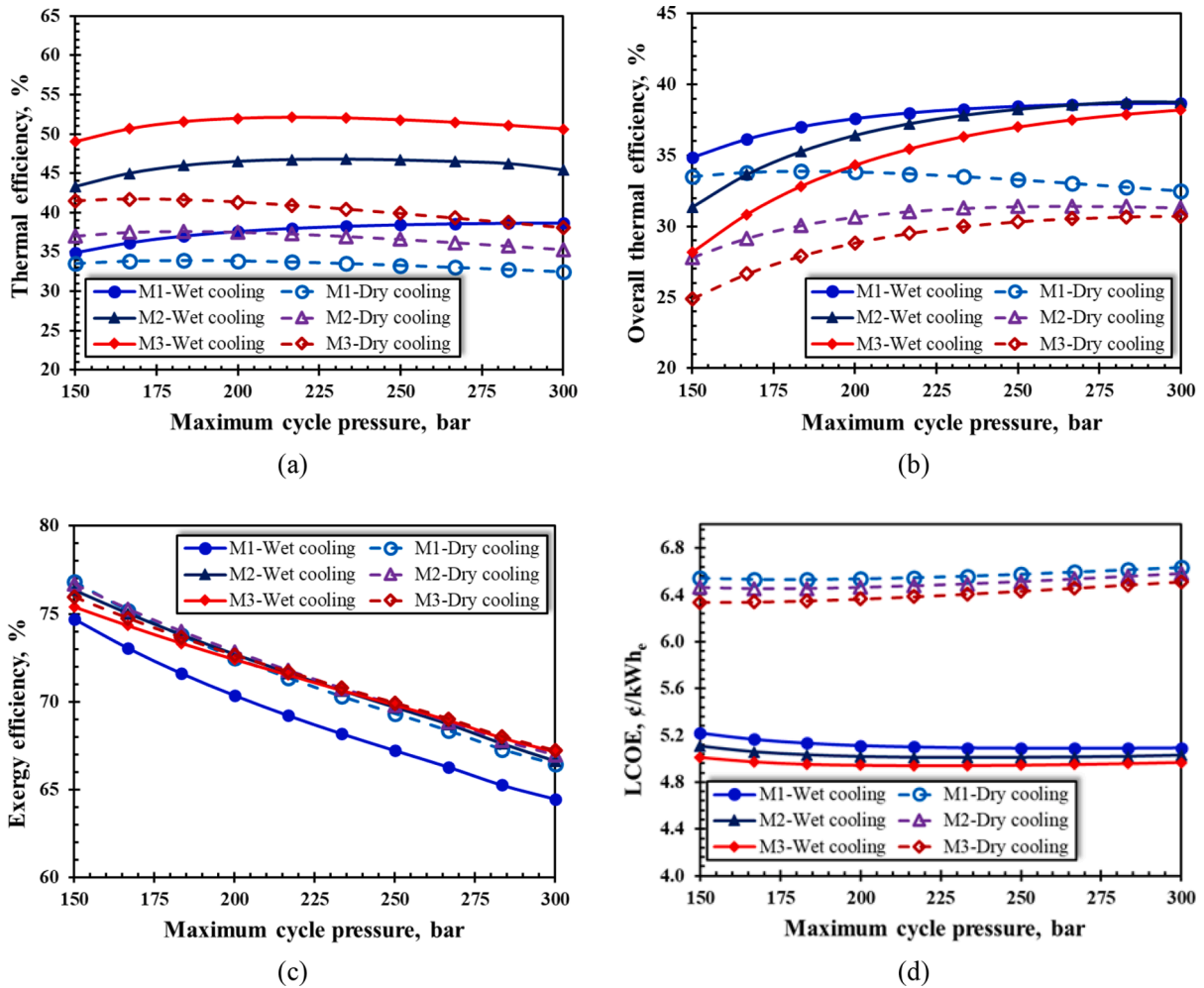
Fig. 8. Split ratio effect on (a) thermal efficiency, (b) overall thermal efficiency, (c) exergy efficiency, and (d) LCOE at wet and dry-cooling conditions.

$\dot{W}_{net}$ from 50MWe to 100MWe reduces the LCOE by a negligible amount of 0.0027¢/MWe. This implies that doubling the power capacity does not double the component capital and operational costs. Moreover, the increase of $\dot{W}_{net}$ improves the heat transfer coefficients of the recuperators, which decreases their costs per MWe plant capacity.

For the exergy efficiency, it can be noted from

Fig. 5(c) that M1 (wet) has the lowest exergy efficiency, while the exergy efficiencies of the other configurations are higher than M1 (wet) by about 3% with only a slight difference from each other.

To analyze the effect of the cooling method and the preheater integration on the exergy performance, it is important to calculate the exergy destruction for each component in each configuration. This exergy destruction portion of each component of the proposed configurations in wet and dry-cooling conditions is shown in Fig. 7(a) to Fig. 7 (f). It can be noted that the exergy destruction portions of the preheater, LTR, and HTR in wet configurations are either equal or higher than in dry configurations, which is attributed to the larger temperature differences occurring through the recuperators in wet-cooling conditions. Furthermore, the exergy destruction portions of the turbomachinery components (GT and GC) are the same for all configurations. On contrary, the exergy destruction portion of the oxy-combustor in M2 and M3 is lower than in M1 by 6% (wet) and 5% (dry). This reduction is achieved by the integration of the preheater, which enhances the temperature of the recycled sCO$_2$ at the combustor inlet and minimizes the exergy destruction across the oxy-combustor. On the other hand, the exergy destruction of the precooler in M2 and M3 is higher than in M1 due to

the increase of the temperature at its inlet. Furthermore, the exergy destruction of the dry precooler is higher than that of the wet precooler as a result of the larger temperatures at the terminals of the dry precooler. In general, the exergy performance of the dry-cooling configurations is higher than that of the wet-cooling configurations by less than 1%. This occurs mainly because of the large temperature difference between the hot and cold streams of the recuperators in wet-cooling conditions compared to those of the dry-cooling conditions.

From the above results, it is found that the increase of T_{max} from 550 °C to 750 °C, enhances the thermal efficiency at least by 10.97% (in wet cooling) and by 9.23% (in dry cooling) for all cases. As a comparison, for a solar-based sCO$_2$ power cycle presented by Ma et al. [65], the increase of T_{max} from 550 °C to 700 °C, improved the thermal efficiency of the cycle by only 9.04% (in wet cooling) and by 5.88% (in dry cooling). This implies that the DOC-based sCO$_2$ power cycles proposed in this study are more efficient compared to the cycle proposed by Ma et al. [65] for both wet and dry cooling methods.

4.3. Effect of the maximum cycle pressure

Fig. 8 shows the effects of the maximum cycle pressure (P_h) on the a) thermal efficiency, b) overall thermal efficiency, c) exergy efficiency, and d) LCOE of the proposed configurations in both wet and dry-cooling conditions.

From Fig. 8(a), the thermal efficiency increases with the increase of P_h up to optimal value then decreases at higher pressures. This returns to
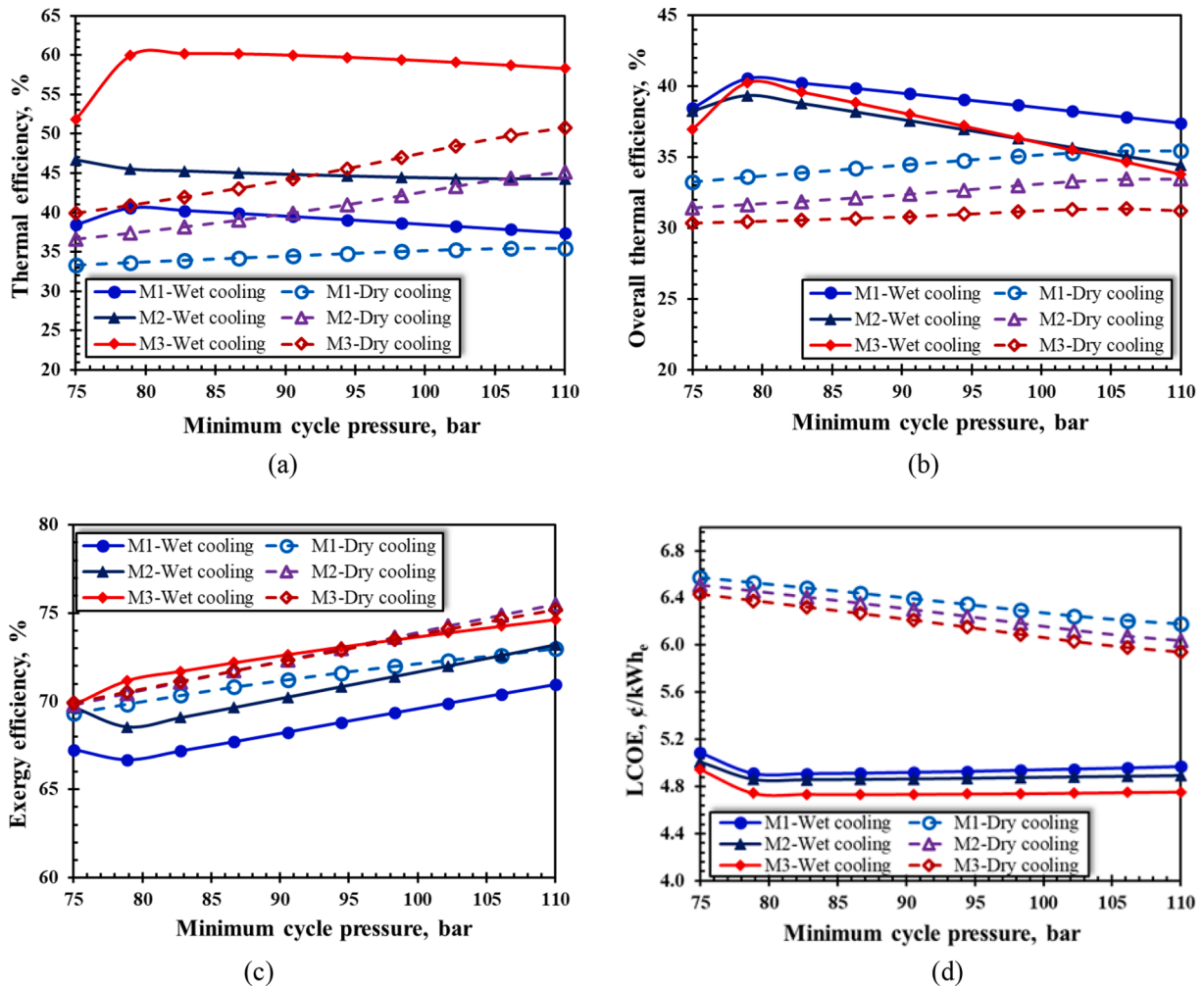
Fig. 9. Minimum cycle pressure effect on (a) thermal efficiency, (b) overall thermal efficiency, (c) exergy efficiency, and (d) LCOE at wet and dry-cooling conditions.

that the increase of the generated power by the GT is higher than that consumed by GC up to the optimal value of the P_h. The opposite is true for P_h higher than the optimal value. Furthermore, due to the dense behavior of the sCO$_2$ in wet cooling, the optimal values of P_h of the dry configurations are lower than those of the wet configurations. For instance, the optimal P_h for M3 (dry) is 183 bar while for M3 (wet) is 216 bar. However, the optimal thermal efficiency of M3 (wet) is 52.10% while for M3 (dry) is 41.62%. This explains the large difference in the LCOE between the dry and wet-cooling configurations as shown in Fig. 8 (d). The optimal values of P_h for the overall thermal efficiency (as shown in Fig. 8(b)) are larger than for the thermal efficiency. Furthermore, the gap between the overall thermal efficiency curves decreases as P_h increases. Lower pressures at the outlet of the GC yields lower temperatures and higher specific heats for the sCO$_2$, thus more heat is required from the preheater. Therefore, the overall thermal efficiency of M1 (dry) is higher than of M3 (wet) at less than $200P_h$ bar and higher than M2 (wet) at less than $166P_h$ bar. This due to that the preheater contribution at these low pressures is more than the reduction achieved in the oxy-combustor load.

In contrast to T_{max} effect, the increase of P_h decreases the overall exergy efficiency of the cycle as shown in Fig. 8(c). This returns to that the increase of P_h increases the temperature at the compressor outlet, which in turn reduces the recuperative heat by the recycled sCO$_2$ and increases the temperature at the inlet of the precooler. This also dictates larger heat transfer areas for the recuperators, which increases the LCOE

at P_h higher than the optimal value for each configuration.

4.4. Effect of the minimum cycle pressure

Fig. 9 shows the effect of the minimum cycle pressure P_l (at the GC inlet) on the a) thermal efficiency, b) overall thermal efficiency, c) exergy efficiency, and d) LCOE for both wet and dry-cooling configurations. From Fig. 9(a) and Fig. 9(b), it can be seen that the efficiency of the wet-cooling configurations is increased with P_l up to $P_l = 78.90$ bar then decreases at higher P_l values. But, in the dry-cooling configurations, the efficiencies increase over the whole range of P_l. This is caused by that, at fixed high pressure of 250 bar, the increase of P_l reduces the pressure ratio towards the optimal value for the dry configurations and far from the optimal values for the wet-cooling configurations. Moreover, the increase of P_l reduces the temperature difference across the compressor, which enhances the performance of the recuperators and yields higher temperatures at the inlet of the combustor. Thus, the temperature differences increase across the recuperators and reduce across the GT and the GC. As an overall result, the increase of the lower pressure improves the exergy efficiency of all configurations as shown in Fig. 9(c).

As a comparison, the effect of P_l on the overall efficiency of six solar-based sCO$_2$ power cycles was investigated by Wang et al. [8] within the range of 74 bar to 90 bar at T_{min} of 35 °C and P_h of 250 bar. Among these configurations, only the recompression layout shows an increase in the
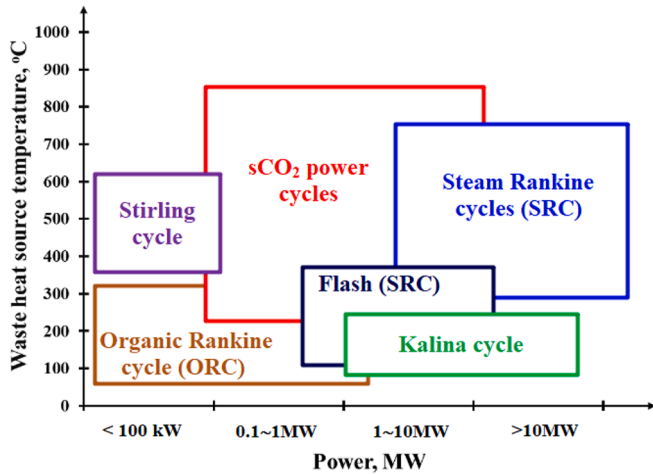
Fig. 10. Waste heat recovery technologies based on the waste heat source temperature and potential power.

Table 5
Examples of waste heat sources that are applicable for the proposed configurations in this study.

#	$\dot{m}_{17}$	T_{17}	Application
	kg/s	°C	
1	80	268	Diesel engine 8S90ME-C10.2 [67]
2	63	572	Shipboard gas turbine engine [68]
3	54	490	Offshore gas turbine [69]
4	138	471	Gas turbine unit (GE LM6000 PH Exhaust) [70]
5	178	680	Gas turbine cycle [64]
6	80	380	Exhaust gas from cement industry [71]

overall efficiency from 29.0% (at $P_l = 74$ bar) up to 30.4% (at 82 bar) then decreases to 29.6% (at $P_l = 90$ bar). In the present study, for the wet cooling configurations, the overall efficiency increases from 36.8% (at $P_l = 75$ bar) up to 40.3% (at $P_l = 78.8$ bar) then decreases to 39.5% (at $P_l = 90$ bar). This indicates that the present cycles with wet cooling configurations are more efficient than the solar-based sCO$_2$ cycles for the same P_l.

4.5. Effect of the waste heat source specifications

Waste heat sources are available at different temperature ranges for which various cycles can be utilized to provide the desired potential power ranges as shown in Fig. 10. The waste heat is localized in each sector (transportation, industrial or power generation). However, each sector has different temperature range of waste heat and different potential utilization methods of this heat. Typically, medium-grade waste heat is around 40 % of all temperature range waste heat [66]. The considered waste heat sources for the presented cycle layouts can be utilized from various sources of medium-grade waste heat such as those shown in Table 5.

However, several factors make waste heat recovery very difficult, such as the operating principle of heat recovery facilities, user demand, and characteristics of the source of the waste heat. From a technical point of view, waste heat sources are subjected to more fluctuation and intermittence than conventional heat sources, which affect the operation stability of the recovery system. Therefore, the development of a proper control strategy of the split process in M2 and M3 can avoid large fluctuations in the performance of the system. Furthermore, the waste heat sources are usually dispersed geographically, which makes it challenging to integrate the recovery system with the original industrial process. In these cases, additional problems like the pressure drop of the flue gases in the heat carrier must be considered.

From an economic point of view, the characteristics of the waste heat sources such as the available temperature and mass flow rate must be sufficient to realize low LCOE in M2 and M3 compared to M1. For instance, the samples of the waste heat sources presented in Table 5 were applied for M2 and M3 configurations in dry and wet cooling conditions. The major results are reported in Table 6. At waste heat temperature of 380 °C (source #6 in Table 5), and mass flow rate of 80 kg/s, the overall efficiency and LCOE are 39.76% and 6.31 ¢/kWh$_e$, respectively in M2 (dry cooling) and 47.44% and 5.37 ¢/kWh$_e$ in M3 (wet cooling). At waste heat temperature of 680 °C (source #5), and mass flow rate of 178 kg/s, the overall efficiency and LCOE are 43.43% and 5.46 ¢/kWh$_e$, respectively in M2 (dry cooling) and 51.71% and 4.23 ¢/kWh$_e$ in M3 (wet cooling). This implies that the cooling conditions and the configuration of the system significantly affect the energetic and economic performances of the proposed cycles. This is explained more by investigating the effect of the waste heat source temperature ranging from 300 °C to 700 °C at a mass flow rate of 80 kg/s for flue gases. The results of this investigation are presented in Fig. 11, where at higher waste heat source temperatures, the preheater share increases and the fuel consumption reduces. This significantly enhances the overall efficiency by an average of 11% and reduces the LCOE by 1.43 ¢/kWh$_e$ over the range of the waste heat source temperature. Furthermore, the overall efficiency in wet cooling conditions is about 7% higher than in dry cooling conditions. This is because the inlet temperature of the recycled sCO$_2$ in wet cases is lower than in dry cases, which enhances the amount of heat recovery from the waste heat sources.

Table 6
Simulation results of the waste heat sources presented in Table 5 in dry and wet conditions of M2 and M3.

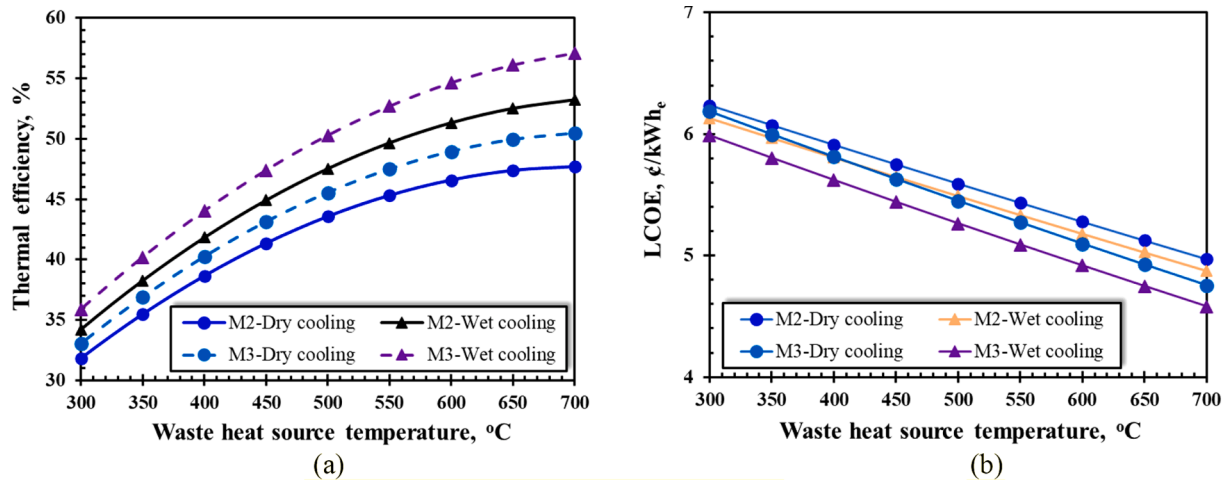| #	Dry cooling							
	M2				M3			
	$\eta_{th,overall}$, %	LCOE, ¢/kWh$_e$	$\dot{m}_f$, kg/s	$\dot{W}_{net}$, MW	$\eta_{th,overall}$, %	LCOE, ¢/kWh$_e$	$\dot{m}_f$, kg/s	$\dot{W}_{net}$, MW
1	37.64	10.50	0.457	12.41	39.12	9.43	0.866	20.41
2	42.51	5.80	1.498	45.99	44.19	5.22	2.840	75.62
3	41.64	6.84	1.040	31.27	43.28	6.15	1.971	51.41
4	40.72	5.65	1.778	52.28	42.33	5.09	3.370	85.96
5	43.34	5.46	1.661	51.99	45.05	4.91	3.149	85.49
6	39.76	6.31	0.989	28.40	41.32	5.57	1.876	46.70
Wet cooling								
1	42.89	7.76	0.622	20.20	44.91	7.04	1.198	33.22
2	48.43	4.89	1.461	53.64	50.72	4.68	2.816	88.20
3	47.44	5.70	1.047	37.64	49.68	5.18	2.018	61.89
4	46.40	4.70	1.807	63.55	48.59	4.27	3.483	104.49
5	49.38	4.66	1.577	59.03	51.71	4.23	3.040	97.06
6	45.30	5.91	1.076	36.95	47.44	5.37	2.074	60.75

Fig. 11. Waste heat source temperature effect on (a) thermal efficiency, and (b) LCOE at wet and dry-cooling conditions.

Table 7
Results of the optimization analysis.

| Cooling method	Mode	Objective function	Decision variables				Optimized results		
			P_h, bar	P_l, bar	T_{max}, °C	S_r	η_{th}, %	$\varepsilon_{overall}$, %	LCOE, ¢/kWh$_e$
Wet-cooling	M1	Max.η_{th}	291.1	77.78	750	1.000	45.65	76.27	5.386
		Max.$\varepsilon_{overall}$	300.0	75.38	550	1.000	37.39	73.78	5.593
		Min. LCOE	283.4	83.72	750	1.000	45.52	76.67	5.386
		Max.MOF	205.6	104.00	716	1.000	41.80	73.26	4.907
	M2	Max.η_{th}	296.4	78.33	750	0.697	45.68	74.21	5.367
		Max.$\varepsilon_{overall}$	296.7	75.00	550	0.800	37.44	73.45	5.568
		Min. LCOE	300.0	90.75	750	0.600	45.46	74.48	5.363
		Max. MOF	250.0	75.00	650	0.730	57.18	74.76	4.828
	M3	Max.η_{th}	293.6	104.6	750	0.600	49.44	73.33	5.165
		Max.$\varepsilon_{overall}$	300.0	78.75	550	0.797	38.90	72.75	5.521
		Min. LCOE	240.0	92.48	750	0.600	49.29	74.04	5.163
		Max.MOF	250.0	75.00	650	0.730	62.19	72.04	**4.677**
Dry-cooling	M1	Max.η_{th}	299.8	86.97	750	1.000	44.06	74.60	6.802
		Max.$\varepsilon_{overall}$	300.0	75.00	550	1.000	34.78	72.71	6.894
		Min. LCOE	296.7	91.01	750	1.000	43.68	77.73	6.561
		Max.MOF	283.3	76.94	583	1.000	41.12	73.63	6.316
	M2	Max.η_{th}	298.3	83.85	750	0.729	43.81	75.40	6.538
		Max.$\varepsilon_{overall}$	299.1	75.24	550	0.797	34.83	73.61	6.865
		Min. LCOE	247.1	75.34	750	0.604	43.66	75.00	6.532
		Max.MOF	283.3	76.94	583	0.700	40.03	71.98	6.307
	M3	Max.η_{th}	277.1	102.4	750	0.605	47.46	75.13	6.282
		Max.$\varepsilon_{overall}$	292.5	76.76	550	0.800	36.17	73.78	6.792
		Min. LCOE	221.8	89.21	750	0.600	47.38	75.12	6.279
		Max.MOF	283.3	76.94	583	0.633	47.75	70.55	**6.139**
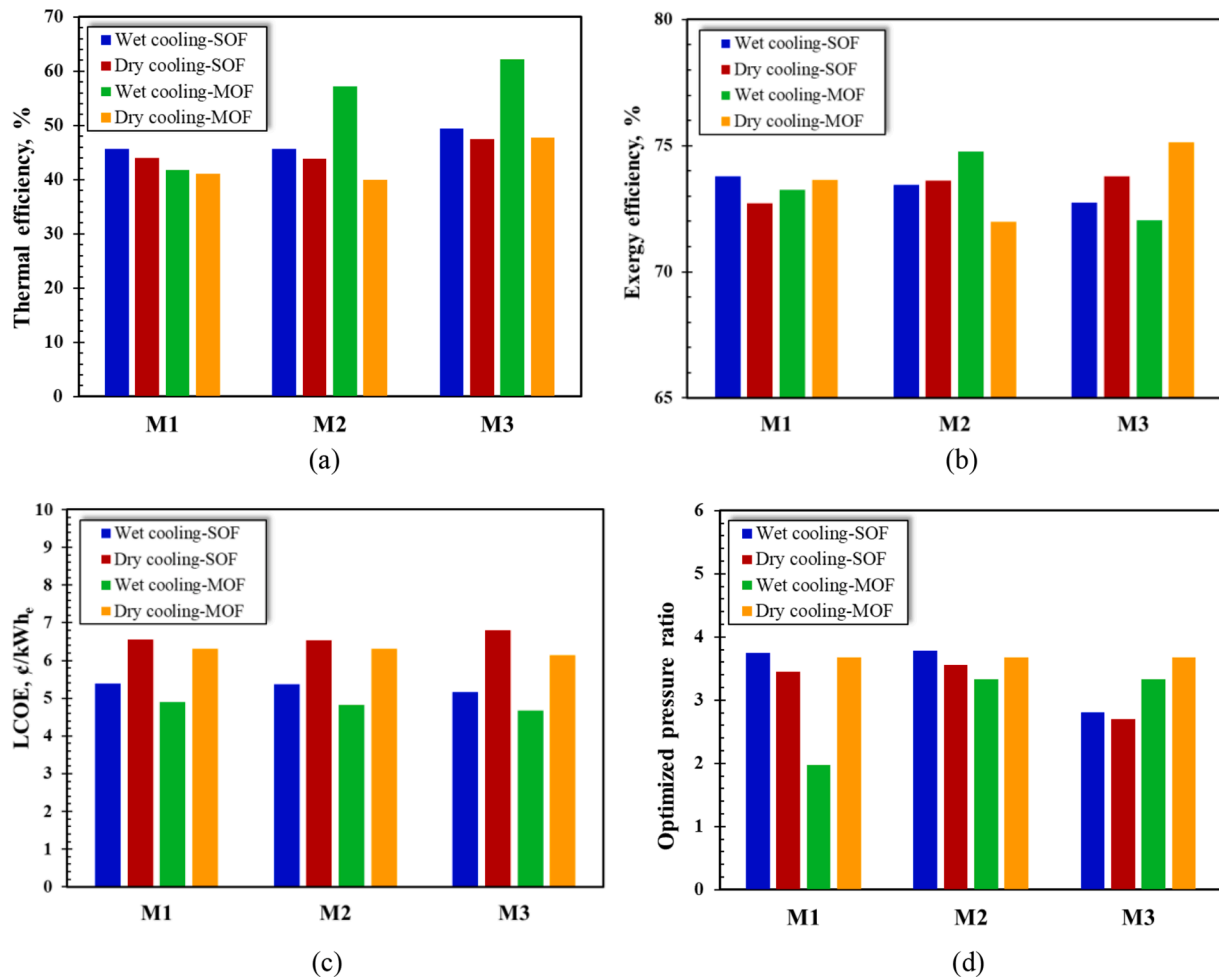
Fig. 12. Single- and multi-objective function (SOF and MOF) optimized results of (a) thermal efficiency, (b) exergy efficiency, (c) LCOE, and d) pressure ratio in both wet and dry conditions.
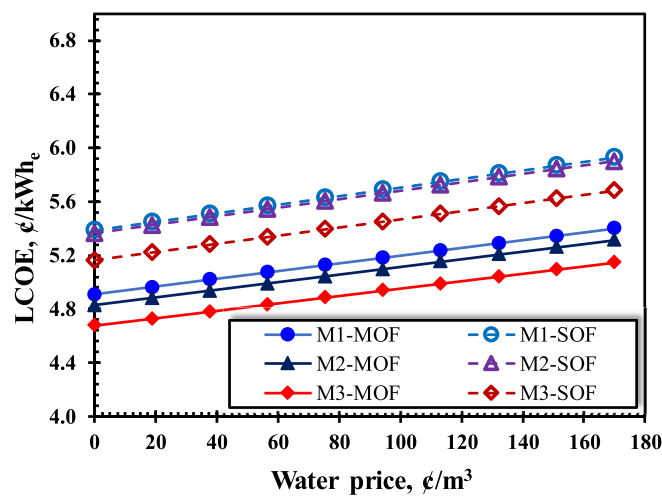

Fig. 13. Effect of water price on LCOE of the wet-cooling configurations obtained by SOF(Min. LCOE) and MOF(Max. MOF).

Table 8

Comparison of LCOE of the proposed configurations with LCOE of other sCO$_2$ power cycles.

Energy source	Configuration	Conditions of the sCO$_2$ power cycle					LCOE, ¢/kWh$_e$	Ref.
		T$_{max}$, °C	T$_{min}$, °C	$\dot{W}_{net}$, MW	P$_h$, bar	P$_l$, bar		
Methane + waste heat	sCO$_2$ power cycle + preheater	650	32	50	250	75.0	4.68	Present study
Methane	Gas turbine cycle + sCO$_2$ power cycle + ORC	873	40	21	249	93.4	5.28	[64]
Methane	Allam cycle	1150	20	846	300	30.0	10.16	[73]
Natural gas	NG-Net Power Allam cycle	–	–	–	–	–	4.00	[74]
Solar energy	Molten salt power tower system + sCO$_2$ recompression cycle	630	45	115	250	105.0	14.38	[75]
Solar energy	Molten salt power tower system + sCO$_2$ recompression cycle	600	35	100	250	68	17.600	[65]

4.6. Optimization analysis

As discussed above, there are considerable differences between the optimal operating conditions of each configuration. Therefore, an optimization analysis is important for the key decision variables that yield high energetic and exergetic efficiencies and low LCOE. For this purpose, the genetic algorithm is used for single- and multi-objective optimization analysis of each cycle configuration. For the single-objective function (SOF) optimization analysis, the objective functions are: maximizing the thermal efficiency (η_{th}), maximizing the overall exergy efficiency ($\varepsilon_{overall}$), and minimizing the LCOE. For the multi-objective function (MOF) optimization analysis, the objective function is defined by assigning a weighting coefficient for each objective function as follows:

$$Max.MOF = w_1 \times \eta_{th} + w_2 \times \varepsilon_{overall} + w_3 \times (1 - \frac{LCOE}{C_{fuel}}) \qquad (23)$$

where w_1, w_2, and w_3 are the weighting coefficients for η_{th}, $\varepsilon_{overall}$, and LCOE, respectively, and in the fuel cost which is 7 ¢/kWh$_e$ [72]. Considering that the three objective functions have the same importance, the weighting coefficients are assumed to be the same ($w_1 = w_2 = w_3 = 1/3$) [59].

The results for the single-objective and multi-objective optimization analysis are provided in Table 7 for both wet and dry-cooling configurations for the following ranges of the decision variables:

$$150 \leq P_h(bar) \leq 300$$

$$75 \leq P_l(bar) \leq 110$$

$$550 \leqslant T_{max}(°C) \leqslant 750$$

$$0.2 \leq S_r \leq 0.8 \ (for \ M2 \ and \ M3)$$

4.6.1. Optimization results

Fig. 12 shows the results obtained by the single-objective functions (SOFs) *Max. η_{th}* (Fig. 12(a)), *Max. $\varepsilon_{overall}$* (Fig. 12(b)), and *Min.LCOE* (Fig. 12(c)) alongside those obtained by the MOF (*Max.MOF*). As can be seen from Table 5 and Fig. 12(a), η_{th} obtained by the MOF is lower than that obtained by the SOF in both wet and dry-cooling scenarios. However, the MOF provides lower LCOE than the SOF as shown in Fig. 12(c). This is because the optimized P_h and P_l provided by the MOF yield a low-pressure ratio in the wet-cooling configurations and a high-pressure ratio for the dry-cooling configurations (see Fig. 12(d)). For instance, the optimized P_h by the SOF (*Max. η_{th}*) for M1 (wet) is higher than the optimized by the MOF (*Max.MOF*) by 27%, while the optimized P_l by the MOF is higher than optimized by the SOF by 25% (Table 7, wet-cooling,

M1 part)). Furthermore, T_{max} that is obtained by the MOF (716 °C) for M1 (wet) is lower than provided by the SOF (750 °C) which yields lower LCOE by the MOF (4.907 ¢/kWh$_e$) compared to the SOF (5.386 ¢/kWh$_e$). Thus, the higher η_{th} obtained by the SOF (45.65%) is caused by the higher T_{max} which, at the same time, increases the components layouts and increases the LCOE. On the other hand, as shown in Table 7 (dry-cooling, M1 part)) the optimized P_h by the SOF (*Max. η_{th}*) for M1 (dry) is higher than the optimized by the MOF (*Max.MOF*) by 5.8% and the optimized P_l is higher by 13%. Moreover, T_{max} obtained by the MOF (583 °C) for M1 (dry) is lower than the provided by the SOF (750 °C), which yields lower LCOE by the MOF (6.802 ¢/kWh$_e$) compared to the SOF (6.316 ¢/kWh$_e$). Therefore, the MOF efficiently provides values for the decision variables that give the minimum LCOE with competitive energy and exergy efficiencies.

The results of the SOF (*Max. $\varepsilon_{overall}$*) do not yield the maximum $\varepsilon_{overall}$ compared to that obtained by the other SOFs for all configurations (see Table 7). However, this function provides high exergy efficiency at T_{max} of 550°C, which is the minimum value obtained compared to the results of the other functions. Also, the LCOE provided by *Max. $\varepsilon_{overall}$* function is higher than obtained by the other functions. Similarly, the LCOE obtained by the *Min. LCOE* function is higher than obtained by the *Max. MOF* function. This implies that the MOF is more efficient than the SOFs in the determination of the optimized decision variables and provides the minimum LCOE for each configuration with comparable energy and exergy efficiencies for those obtained by the SOFs.

Comparing the results of the MOF for M2 and M3 relative to M1 (Table 7, wet-cooling), it can be seen that a minimum LCOE of 4.677 ¢/kWh$_e$ is obtained for M3 at $T_{max} = 650°C$, $P_h = 250$ bar, $P_l = 75$ bar, and $S_r = 0.73$. For the dry-cooling configurations, a minimum LCOE of 6.139 ¢/kWh$_e$ is obtained for M3 at $T_{max} = 583°C$, $P_h = 283$ bar, $P_l = 77$ bar, and $S_r = 0.63$. Also, the η_{th} is maximum at these conditions with 62.19% for M3 (wet) and 47.75% for M3 (dry) with overall exergy efficiency of 72.04% for M3 (wet) and 70.55% for M3 (dry). Therefore, to maximize both the η_{th} and $\varepsilon_{overall}$, and to minimize the LCOE, high T_{max} at low-pressure ratios are recommended for the wet-cooling configurations and low T_{max} at high-pressure ratios are recommended for the dry-cooling configurations.

4.6.2. Effect of water cost

In arid and desert regions, the water scarcity makes its cost higher than usual and thus the prices of water could impact the LCOE for wet-cooling configurations. Fig. 13 shows the results of incorporating the water price into the LCOE of the wet-cooling configurations. Taking the range of the water price to be (0–1.7 $/m^3) [56,57], the LCOE linearly increases from 5.163¢/kWh$_e$ to 5.68¢/kWh$_e$ (for M3-SOF) and from 4.677¢/kWh$_e$ to 5.146¢/kWh$_e$ (for M3-MOF). Therefore, at a water

price of 170¢/kWh$_e$, the difference between the LCOE of the dry and wet-cooling configurations reduces from 1.462¢/kWh$_e$ (without water price) to 0.459¢/kWh$_e$ (at a water price of 170¢/m^3). However, it was found that when the water price reaches 277¢/m^3, then the LCOE of M3 (wet) will be the same as the LCOE of M3 (dry). This implies that a further increase in the water price makes the dry-cooling configurations a better option than the wet-cooling configurations from an economic point of view.

4.6.3. LCOE comparison

Table 8 presents a comparison between the optimized LCOE of configuration M3 (wet) of the present study with the LCOE for other sCO$_2$ power cycles available in the literature. It can be seen that the LCOE of the Allam cycle is higher than the other cycles that use methane as an energy source. However, based on the future advances on the sCO$_2$ power systems, the LCOE of the natural gas net power Allam cycle is expected to be 4 ¢/kWh$_e$ as presented by Wright and Anderson [74]. The LCOE of the sCO$_2$ cycles that are driven by the molten salt power tower system is about three times higher than those driven by methane with less than $900 T_{max}°$C. This returns to the high capital investment of the solar tower system. Furthermore, the high temperature and pressure at the turbine inlet of the Allam cycle increase the complexity (and certainly the cost) of the cycle component. The LCOE for M3 configuration of the present study is the minimum compared to the other available in literature configurations, which makes it attractive for future sCO$_2$ power cycles.

5. Conclusions

Thermoeconomic and optimization analyses have been conducted for three direct oxy-fuel sCO$_2$ power cycles that operate at moderate turbine inlet temperatures (550–750 °C) in wet- and dry-cooling conditions. The first cycle, M1 is a typical direct oxy-fuel sCO$_2$ power cycle and is used for comparison with the other two cycles M2 and M3. The second cycle, M2 integrates a preheater in parallel with the LTR while the third cycle, M3 integrates a preheater in parallel with both the LTR and HTR. This integration of the preheater improves the thermal efficiency of the cycle and reduces the LCOE by minimizing the consumed fuel by the combustor. Furthermore, the preheater improves the performance of the LTR by eliminating the thermodynamic imbalance without reducing the flexibility of the system. Moreover, the preheater simplifies the design of the cycle recuperators by reducing their heat transfer areas and thus reduces their costs and the LCOE. Thorough energetic, exergetic, and economic models were developed and validated to evaluate the performance of the proposed configurations in terms of the energy and exergy efficiencies, and the LCOE. Then, the performance of each cycle was optimized by conducting single- and multi-objective optimization analyses. All of these analyses were performed for each cycle and compared in both wet and dry-cooling conditions. The main conclusions of this study are summarized as follows:

- The integration of the preheater improves the thermal efficiency of M2 (by 5.81% (wet), and 3.27% (dry)), and M3 (by 13.27% (wet), and 6.58% (dry) compared to M1.
- The LCOE of M1 (without preheater) is higher than of M2 (by 10.8% (wet), and 5.7% (dry)), and higher than of M3 (by 19.1% (wet), and 11.4% (dry)).
- The overall exergy efficiency of the wet-cooling configurations is slightly lower than of the dry-cooling due to the larger temperature differences across the recuperators of the wet configurations. While

this enhances the energy performance of the recuperators, it is negatively affecting the exergy efficiency of the recuperators and the combustor.
- At $T_{max} = 650$ °C, the increase of the net output power from 50 MW to 100 MW reduces the LCOE by 0.0027¢/MW$_e$ in both wet and dry-cooling conditions.
- The optimization results tend toward higher turbine inlet temperatures with low-pressure ratios for wet-cooling configurations and lower turbine temperatures with high-pressure ratios for the dry-cooling configurations.
- A minimum LCOE of 4.667¢/kWh$_e$ is obtained by the multi-objective optimization for M3 (wet) and of 6.139¢/kWh$_e$ for M3 (dry).
- At water prices of 277¢/m^3, the LCOE of M3 (wet) will be the same as the LCOE of M3 (dry).

Future work of the present layouts may include the following perspectives:

- Investigating the present layouts with liquefied natural gas (LNG) as a fuel source instead of conventional natural gas. The cold energy of LNG can be used to minimize the compression power of the recycled sCO$_2$, which further improves the efficiency of the system.
- As the intercooled sCO$_2$ power cycles investigated in the literature introduce a completive energy efficiency for the recompression sCO$_2$ power cycles, the present layouts should be studied with multi-intercooled compression stages and compared with the results presented in this study.
- Detailed part-load with proper control strategies need to be developed to adjust the cycle load and performance at off-design conditions with a focus on the off-design conditions of the waste heat source.

CRediT authorship contribution statement

Ahmad K. Sleiti: Conceptualization, Investigation, Writing – original draft, Writing - review & editing, Project administration, Funding acquisition, Formal analysis, Supervision, Visualization. **Wahib A. Al-Ammari:** Conceptualization, Writing – original draft, Data curation, Software, Visualization. **Ladislav Vesely:** Conceptualization, Writing - review & editing, Visualization. **Jayanta S. Kapat:** Conceptualization, Supervision, Visualization.

Declaration of Competing Interest

The authors declare that they have no known competing financial interests or personal relationships that could have appeared to influence the work reported in this paper.

Acknowledgement

Appendix

Table A1
State points of the proposed configurations (M1, M2, and M3) at the design point parameters of the wet and dry cooling conditions.

Cycle	State	Wet cooling					Dry cooling				
		T	P	$\dot{m}$	h	s	T	P	$\dot{m}$	h	s
		°C	bar	kg/s	kJ/kg	kJ/kg-°C	°C	bar	kg/s	kJ/kg	kJ/kg-°C
M1	1	750	237	407	779	0.241	750	237	509	779	0.241
	2	590	81	407	586	0.245	590	81	509	586	0.245
	3	442	79	407	410	0.027	507	79	509	486	0.129
	4	149	78	407	76	−0.571	178	78	509	109	−0.497
	5	32	76	407	−144	−1.206	50	76	509	−61	−0.939
	6	32	75	400	−144	−1.206	50	75	501	−61	−0.939
	7	99	250	400	−106	−1.196	153	250	501	2.32	−0.924
	8	–	–	–	–	–	–	–	–	–	–
	9	–	–	–	–	–	–	–	–	–	–
	10	317	247	400	234	−0.459	438	247	501	386	−0.225
	11	460	245	400	413	−0.186	520	245	501	488	−0.088
	12	25	10	2.44	−9.8	−1.211	25	10	2.73	−9.8	−1.211
	13	327	245	2.44	784	−1.076	327	245	2.73	784	−1.076
	14	25	1	42.0	298	6.864	25	1	46.9	298	6.864
	15	25	10	9.77	−2.5	−0.602	25	10	11	−2.5	−0.602
	16	427	245	9.77	1146	7.363	427	245	11	1146	7.363
	a	27	3	197	105	0.464	–	–	–	–	–
	b	140	2.9	197	2740	1.738	–	–	–	–	–
	c	22	1	197	104	0.464	–	–	–	–	–
M2	1	750	237	407	779	0.241	750	237	509	779	0.241
	2	590	81	407	586	0.245	590	81	509	586	0.245
	3	506	79	407	486	0.129	489	79	509	465	0.102
	4	200	78	407	133	−0.444	276	78	509	220	−0.274
	5	32	76	407	−144	−1.206	50	76	509	−61	−0.939
	6	32	75	400	−144	−1.206	50	75	501	−61	−0.939
	7	99	250	400	−105	−1.196	153	250	501	2.32	−0.925
	8	99	250	108	−105	−1.196	153	250	135	2.32	−0.925
	9	350	247	108	275	−1.984	350	247	135	275	−0.391
	10	438	247	292	386	−0.459	405	247	366	345	−0.285
	11	550	245	400	525	−0.186	540	245	501	513	0.057
	12	25	10	2.06	−9.8	−1.211	25	10	2.49	−9.8	−1.211
	13	327	245	2.06	784	−1.076	327	245	2.49	784	−1.076
	14	25	1	35.4	298	6.864	25	1	42.8	298	6.864
	15	25	10	8.2	−2.5	−0.062	25	10	9.9	−2.5	−0.602
	16	427	245	8.2	1146	−0.519	427	245	9.9	1146	−0.519
	17	370	5	159	339	−0.518	370	5	179	339	−0.518
	18	119	4.4	159	81	−0.060	173	4.9	179	133	−0.060
	a	27	3	41.2	105	0.367	–	–	–	–	–
	b	190	2.9	41.2	2844	7.036	–	–	–	–	–
	c	25	1	41.2	104	0.367	–	–	–	–	–
M3	1	750	237	407	779	0.241	750	237	509	779	0.241
	2	590	81	407	586	0.245	590	81	509	586	0.245
	3	524	79	407	506	0.155	541	79	509	527	0.180
	4	191	78	407	124	−0.463	252	78	509	192	−0.325
	5	32	76	407	−144	−1.206	50	76	509	−61.1	−0.940
	6	32	75	400	−144	−1.206	50	75	501	−61.1	−0.940
	7	99	250	400	−105	−1.196	153	250	501	2.32	−0.925
	8	99	250	108	−105	−1.196	153	250	135	2.32	−0.925
	9	520	247	108	488	−0.090	520	247	135	488	−0.090
	10	471	247	292	427	−0.168	504	247	366	469	−0.115
	11	560	245	292	538	−0.026	570	245	366	550	−0.011
	12	25	10	1.85	−9.8	−1.211	25	10	2.27	−9.8	−1.211
	13	327	245	1.85	784	−1.076	327	245	2.27	784	−1.076
	14	25	1	31.82	298	6.864	25	1	39.1	298	6.864
	15	25	10	7.4	−2.5	−0.602	25	10	9.1	−2.51	−0.602
	16	427	245	7.4	1146	−0.519	427	245	9.1	1146	−0.519
	17	540	5	142	533	−0.518	540	5	164	533	−0.518
	18	119	4.9	142	81	−0.602	173	4.9	164	133	0.066
	a	27	3	40	105	0.367	–	–	–	–	–
	b	182	2.9	40	2828	7.24	–	–	–	–	–
	c	25	1	40	104	0.367	–	–	–	–	–

References

[1] Ritchie H. Energy. Our World Data 2014. https://ourworldindata.org/energy.

[2] U.S. Energy Information Administration. Annual Energy Reviews n.d.

[3] EIA. EIA projects nearly 50% increase in world energy usage by 2050, led by growth in Asia 2020.

[4] Wang J, Sun T, Zeng X, Fu J, Zhao J, Deng S, et al. Feasibility of solar-assisted CO2 capture power plant with flexible operation: A case study in China. Appl Therm Eng 2021;182:116096. https://doi.org/10.1016/j.applthermaleng.2020.116096.

[5] Rissman J, Bataille C, Masanet E, Aden N, Morrow WR, Zhou N, et al. Technologies and policies to decarbonize global industry: Review and assessment of mitigation drivers through 2070. Appl Energy 2020;266:114848. https://doi.org/10.1016/j.apenergy.2020.114848.

[6] Yang J, Yang Z, Duan Y. Off-design performance of a supercritical CO2 Brayton cycle integrated with a solar power tower system. Energy 2020;201:117676. https://doi.org/10.1016/j.energy.2020.117676.

[7] Mohammadi K, Ellingwood K, Powell K. Novel hybrid solar tower-gas turbine combined power cycles using supercritical carbon dioxide bottoming cycles. Appl Therm Eng 2020;178:115588. https://doi.org/10.1016/j.applthermaleng.2020.115588.

[8] Wang K, He YL, Zhu HH. Integration between supercritical CO2 Brayton cycles and molten salt solar power towers: A review and a comprehensive comparison of different cycle layouts. Appl Energy 2017;195:819–36. https://doi.org/10.1016/j.apenergy.2017.03.099.

[9] Wang G, Wang C, Chen Z, Hu P. Design and performance evaluation of an innovative solar-nuclear complementarity power system using the S-CO2 Brayton cycle. Energy 2020;197:117282. https://doi.org/10.1016/j.energy.2020.117282.

[10] McClung A, Brun K, Chordia L. Technical and economic evaluation of supercritical oxy-combustion for power generation. Fourth Supercrit. CO 2 Power Cycles Symp. Pittsburgh, PA, Sept, Pittsburgh, Pennsylvania: 2014, p. 1–14.

[11] Kárászová M, Zach B, Petrusová Z, Červenka V, Bobák M, Šyc M, et al. Post-combustion carbon dioxide capture by membrane separation. Review. Sep Purif Technol 2020;238:116448. https://doi.org/10.1016/j.seppur.2019.116448.

[12] Mukherjee A, Okolie JA, Abdelrasoul A, Niu C, Dalai AK. Review of post-combustion carbon dioxide capture technologies using activated carbon. J Environ Sci (China) 2019;83:46–63. https://doi.org/10.1016/j.jes.2019.03.014.

[13] White MT, Bianchi G, Chai L, Tassou SA, Sayma AI. Review of supercritical CO2 technologies and systems for power generation. Appl Therm Eng 2021;185:116447. https://doi.org/10.1016/j.applthermaleng.2020.116447.

[14] Vega F, Camino S, Camino JA, Garrido J, Navarrete B. Partial oxy-combustion technology for energy efficient CO2 capture process. Appl Energy 2019;253:113519. https://doi.org/10.1016/j.apenergy.2019.113519.

[15] Zhao Y, Chi J, Zhang S, Xiao Y. Thermodynamic study of an improved MATIANT cycle with stream split and recompression. Appl Therm Eng 2017;125:452–69. https://doi.org/10.1016/j.applthermaleng.2017.05.023.

[16] Jericha H, Sanz W, Göttlich E. Design concept for large output Graz Cycle gas turbines. J Eng Gas Turbines Power 2008;130:1–10. https://doi.org/10.1115/1.2747260.

[17] Bolland O, Mathieu PhiliPpe. Comparison of two CO2 removal options in combined cycle power plants. Energy Convers Manag 1998;39(16-18):1653–63. https://doi.org/10.1016/S0196-8904(98)00078-8.

[18] Allam RJ, Fetvedt JE, Forrest BA, Freed DA. The OXY-fuel, supercritical CO2 allam cycle: New cycle developments to produce even lower-cost electricity from fossil fuels without atmospheric emissions. Proc ASME Turbo Expo 2014;GT2014-269:1–9.. https://doi.org/10.1115/GT2014-26952.

[19] Crespi F, Gavagnin G, Sánchez D, Martínez GS. Supercritical carbon dioxide cycles for power generation: A review. Appl Energy 2017;195:152–83. https://doi.org/10.1016/j.apenergy.2017.02.048.

[20] Fernandes D, Wang S, Xu Q, Chen D. Dynamic simulations of the allam cycle power plant integrated with an air separation unit. Int J Chem Eng 2019;2019:325–40. https://doi.org/10.1155/2019/6035856.

[21] Scaccabarozzi R, Gatti M, Martelli E. Thermodynamic analysis and numerical optimization of the NET Power oxy-combustion cycle. Appl Energy 2016;178:505–26. https://doi.org/10.1016/j.apenergy.2016.06.060.

[22] Zhu Q. Innovative power generation systems using supercritical CO2 cycles. Clean Energy 2017. https://doi.org/10.1093/ce/zkx003.

[23] Allam RJ, Palmer MR, Brown GW, Fetvedt J, Freed D, Nomoto H, et al. High efficiency and low cost of electricity generation from fossil fuels while eliminating atmospheric emissions, including carbon dioxide. Energy Procedia 2013;37:1135–49. https://doi.org/10.1016/j.egypro.2013.05.211.

[24] Allam R, Martin S, Forrest B, Fetvedt J, Lu X, Freed D, et al. Demonstration of the allam cycle: an update on the development status of a high efficiency supercritical carbon dioxide power process employing full carbon capture. Energy Procedia 2017;114:5948–66. https://doi.org/10.1016/j.egypro.2017.03.1731.

[25] Rogalev A, Grigoriev E, Kindra V, Rogalev N. Thermodynamic optimization and equipment development for a high efficient fossil fuel power plant with zero emissions. J Clean Prod 2019;236:117592. https://doi.org/10.1016/j.jclepro.2019.07.067.

[26] Zhu Z, Chen Y, Wu J, Zhang S, Zheng S. A modified Allam cycle without compressors realizing efficient power generation with peak load shifting and CO2 capture. Energy 2019;174:478–87. https://doi.org/10.1016/j.energy.2019.01.165.

[27] Chan W, Lei X, Chang F, Li H. Thermodynamic analysis and optimization of Allam cycle with a reheating configuration. Energy Convers Manag 2020;224:113382. https://doi.org/10.1016/j.enconman.2020.113382.

[28] Zaryab SA, Scaccabarozzi R, Martelli E. Advanced part-load control strategies for the Allam cycle. Appl Therm Eng 2020;168:114822. https://doi.org/10.1016/j.applthermaleng.2019.114822.

[29] Yu H, Gundersen T, Gençer E. Optimal liquified natural gas (LNG) cold energy utilization in an Allam cycle power plant with carbon capture and storage. Energy Convers Manag 2021;228:113725. https://doi.org/10.1016/j.enconman.2020.113725.

[30] Rogalev A, Rogalev N, Kindra V, Vegera A, Zonov A. Multi-stream heat exchanger for oxy-fuel combustion power cycle. AIP Conf Proc 2021;2323. https://doi.org/10.1063/5.0041543.

[31] Dokhaee E, Saraei A, Jafari Mehrabadi S, Yousefi P. Simulation of the Allam cycle with carbon dioxide working fluid and comparison with Brayton cycle. Int J Energy Environ Eng 2021;12(3):543–50.

[32] Ong C-W, Chen C-L. Intensification, Optimization and Economic Evaluations of the Oxy-fuel Power Generation with CO2 Capture using the Liquefied Natural Gas Cold Energy. Energy 2021;234:121255. https://doi.org/10.1016/j.energy.2021.121255.

[33] Ferrari N, Mancuso L, Davison J, Chiesa P, Martelli E, Romano MC. Oxy-turbine for Power Plant with CO2 Capture. Energy Procedia 2017;114:471–80. https://doi.org/10.1016/j.egypro.2017.03.1189.

[34] Rodríguez Hervás G, Petrakopoulou F. Exergoeconomic Analysis of the Allam Cycle. Energy Fuels 2019;33(8):7561–8. https://doi.org/10.1021/acs.energyfuels.9b01348.

[35] Chan W, Li H, Li Xi, Chang F, Wang L, Feng Z. Exergoeconomic analysis and optimization of the Allam cycle with liquefied natural gas cold exergy utilization. Energy Convers Manag 2021;235:113972. https://doi.org/10.1016/j.enconman.2021.113972.

[36] Alenezi A, Vesely L, Kapat J. Exergoeconomic analysis of a hybrid sCO2 Brayton power cycle. 4th Eur. sCO2 Conf. Energy Syst. 2021:1–16. https://doi.org/10.17185/duepublico/73980.

[37] Yang H, Li J, Wang Q, Wu L, Reyes Rodríguez-Sanchez M, Santana D, et al. Performance investigation of solar tower system using cascade supercritical carbon dioxide Brayton-steam Rankine cycle. Energy Convers Manag 2020;225:113430. https://doi.org/10.1016/j.enconman.2020.113430.

[38] Atif M, Al-Sulaiman FA. Energy and exergy analyses of solar tower power plant driven supercritical carbon dioxide recompression cycles for six different locations. Renew Sustain Energy Rev 2017;68:153–67. https://doi.org/10.1016/j.rser.2016.09.122.

[39] Elbeih M, Sleiti AK. Analysis and Optimization of Concentrated Solar Power Plant for Application in Arid Climate. J Energy Sci Eng ISSN 2050-0505 2020. doi: ESE-2020-01-0043.

[40] Sleiti AK, Al-Ammari W, Ahmed S, Kapat J. Direct-fired oxy-combustion supercritical-CO2 power cycle with novel preheating configurations -thermodynamic and exergoeconomic analyses. Energy 2021;226:120441. https://doi.org/10.1016/j.energy.2021.120441.

[41] Wu P, Ma Y, Gao C, Liu W, Shan J, Huang Y, et al. A review of research and development of supercritical carbon dioxide Brayton cycle technology in nuclear engineering applications. Nucl Eng Des 2020;368:110767. https://doi.org/10.1016/j.nucengdes.2020.110767.

[42] Shublaq M, Sleiti AK. Experimental analysis of water evaporation losses in cooling towers using filters. Appl Therm Eng 2020;175:115418. https://doi.org/10.1016/j.applthermaleng.2020.115418.

[43] Sleiti AK, Al-Khawaja H, Al-Khawaja H, Al-Ali M. Harvesting water from air using adsorption material – Prototype and experimental results. Sep Purif Technol 2021;257:117921. https://doi.org/10.1016/j.seppur.2020.117921.

[44] Lock A, Hooman K, Guan Z. A detailed model of direct dry-cooling for the supercritical carbon dioxide Brayton power cycle. Appl Therm Eng 2019;163:114390. https://doi.org/10.1016/j.applthermaleng.2019.114390.

[45] Duniam S, Veeraragavan A. Off-design performance of the supercritical carbon dioxide recompression Brayton cycle with NDDCT cooling for concentrating solar power. Energy 2019;187:115992. https://doi.org/10.1016/j.energy.2019.115992.

[46] Ladislav V, Vaclav D, Ondrej B, Vaclav N. Pinch point analysis of heat exchangers for supercritical carbon dioxide with gaseous admixtures in CCS systems. Energy Procedia 2016;86:489–99. https://doi.org/10.1016/j.egypro.2016.01.050.

[47] Jin Y, Gao N, Wang T. Influence of heat exchanger pinch point on the control strategy of Organic Rankine cycle (ORC). Energy 2020;207:118196. https://doi.org/10.1016/j.energy.2020.118196.

[48] Li Bo, Wang S-S, Wang K, Song L. Comparative investigation on the supercritical carbon dioxide power cycle for waste heat recovery of gas turbine. Energy Convers Manag 2021;228:113670. https://doi.org/10.1016/j.enconman.2020.113670.

[49] Wu C, Wang S sen, Li J. Exergoeconomic analysis and optimization of a combined supercritical carbon dioxide recompression Brayton/organic flash cycle for nuclear power plants. Energy Convers Manag 2018;171:936–52. https://doi.org/10.1016/j.enconman.2018.06.041.

[50] Tozlu A, Abuşoğlu A, Özahi E. Thermoeconomic analysis and optimization of a Re-compression supercritical CO2 cycle using waste heat of Gaziantep Municipal Solid Waste Power Plant. Energy 2018;143:168–80. https://doi.org/10.1016/j.energy.2017.10.120.

[51] Luo Dan, Huang Diangui. Thermodynamic and exergoeconomic investigation of various SCO2 Brayton cycles for next generation nuclear reactors. Energy Convers Manag 2020;209:112649. https://doi.org/10.1016/j.enconman.2020.112649.

[52] Noaman M, Saade G, Morosuk T, Tsatsaronis G. Exergoeconomic analysis applied to supercritical CO2 power systems. Energy 2019;183:756–65. https://doi.org/10.1016/j.energy.2019.06.161.

[53] Thanganadar D, Asfand F, Patchigolla K. Thermal performance and economic analysis of supercritical Carbon Dioxide cycles in combined cycle power plant. Appl Energy 2019;255:113836. https://doi.org/10.1016/j.apenergy.2019.113836.

[54] Wright S, Scammell W. Economics. Fundam. Appl. Supercrit. Carbon Dioxide Based Power Cycles, 2017, p. 127–45. doi: 10.1016/B978-0-08-100804-1.00006-2.

[55] Weiland NT, Lance BW, Pidaparti SR. SCO2 power cycle component cost correlations from DOE data spanning multiple scales and applications. Proc ASME Turbo Expo 2019;9:1–18. https://doi.org/10.1115/GT2019-90493.

[56] Walraven D, Laenen B, D'haeseleer W. Minimizing the levelized cost of electricity production from low-temperature geothermal heat sources with ORCs: water or air cooled? Appl Energy 2015;142:144–53. https://doi.org/10.1016/j.apenergy.2014.12.078.

[57] Usman M, Imran M, Yang Y, Lee DH, Park BS. Thermo-economic comparison of air-cooled and cooling tower based Organic Rankine Cycle (ORC) with R245fa and R1233zde as candidate working fluids for different geographical climate conditions. Energy 2017;123:353–66. https://doi.org/10.1016/j.energy.2017.01.134.

[58] Ebrahimi A, Meratizaman M, Reyhani HA, Pourali O, Amidpour M. Energetic, exergetic and economic assessment of oxygen production from two columns cryogenic air separation unit. Energy 2015;90:1298–316. https://doi.org/10.1016/j.energy.2015.06.083.

[59] Alharbi S, Elsayed ML, Chow LC. Exergoeconomic analysis and optimization of an integrated system of supercritical CO2 Brayton cycle and multi-effect desalination. Energy 2020;197:117225. https://doi.org/10.1016/j.energy.2020.117225.

[60] Zare V, Mahmoudi SMS, Yari M, Amidpour M. Thermoeconomic analysis and optimization of an ammonia-water power/cooling cogeneration cycle. Energy 2012;47(1):271–83. https://doi.org/10.1016/j.energy.2012.09.002.

[61] Sifat NS, Haseli Y. Thermodynamic modeling of Allam cycle. ASME Int Mech Eng Congr Expo Proc 2018;6A-144113:1–5. doi: 10.1115/IMECE2018-88079.

[62] Zhang N, Lior N, Liu M, Han W. COOLCEP (cool clean efficient power): A novel CO2-capturing oxy-fuel power system with LNG (liquefied natural gas) coldness energy utilization. Energy 2010;35(2):1200–10. https://doi.org/10.1016/j.energy.2009.04.002.

[63] Hou S, Wu Y, Zhou Y, Yu L. Performance analysis of the combined supercritical CO2 recompression and regenerative cycle used in waste heat recovery of marine gas turbine. Energy Convers Manag 2017;151:73–85. https://doi.org/10.1016/j.enconman.2017.08.082.

[64] Mohammadi K, Ellingwood K, Powell K. A novel triple power cycle featuring a gas turbine cycle with supercritical carbon dioxide and organic Rankine cycles: Thermoeconomic analysis and optimization. Energy Convers Manag 2020;220: 113123. https://doi.org/10.1016/j.enconman.2020.113123.

[65] Ma Y, Morosuk T, Luo J, Liu M, Liu J. Superstructure design and optimization on supercritical carbon dioxide cycle for application in concentrated solar power plant. Energy Convers Manag 2020;206:112290. https://doi.org/10.1016/j.enconman.2019.112290.

[66] Forman C, Muritala IK, Pardemann R, Meyer B. Estimating the global waste heat potential. Renew Sustain Energy Rev 2016;57:1568–79. https://doi.org/10.1016/j.rser.2015.12.192.

[67] Feng Y, Du Z, Shreka M, Zhu Y, Zhou S, Zhang W. Thermodynamic analysis and performance optimization of the supercritical carbon dioxide Brayton cycle combined with the Kalina cycle for waste heat recovery from a marine low-speed diesel engine. Energy Convers Manag 2020;206:112483. https://doi.org/10.1016/j.enconman.2020.112483.

[68] Sharma OP, Kaushik SC, Manjunath K. Thermodynamic analysis and optimization of a supercritical CO2 regenerative recompression Brayton cycle coupled with a marine gas turbine for shipboard waste heat recovery. Therm Sci Eng Prog 2017;3: 62–74. https://doi.org/10.1016/j.tsep.2017.06.004.

[69] Zhang Q, Ogren RM, Kong SC. Thermo-economic analysis and multi-objective optimization of a novel waste heat recovery system with a transcritical CO2 cycle for offshore gas turbine application. Energy Convers Manag 2018;172:212–27. https://doi.org/10.1016/j.enconman.2018.07.019.

[70] Moroz L, Burlaka M, Rudenko O, Joly C. Evaluation of gas turbine exhaust heat recovery utilizing composite supercritical CO2 cycle. Proc Int Gas Turbine Congr 2015;2015:7.

[71] Olumayegun O, Wang M. Dynamic modelling and control of supercritical CO2 power cycle using waste heat from industrial processes. Fuel 2019;249:89–102. https://doi.org/10.1016/j.fuel.2019.03.078.

[72] Breeze P. The Cost of Electricity Generation from Natural Gas-Fired Power Plants. Gas-Turbine Power Gener. 2016;93–8. https://doi.org/10.1016/b978-0-12-804005-8.00010-0.

[73] IEAGHG. Oxy-Combustion Turbine Power Plants. Cheltenham, UK: IEAGHG; 2015.

[74] Wright SA, Anderson M. Supercritical CO2 cycle for advanced NPPs. Work New Cross-Cutting Technol Nucl Power Plants 2017:1–25.

[75] Neises T, Turchi C. Supercritical carbon dioxide power cycle design and configuration optimization to minimize levelized cost of energy of molten salt power towers operating at 650 °C. Sol Energy 2019;181:27–36. https://doi.org/10.1016/j.solener.2019.01.078.